

# Adjoint-based Gradient Estimation Using the Space-time Solutions of Unknown Conservation Law Simulations

By Han CHEN<sup>†</sup> AND Qiqi WANG<sup>†</sup>

Many control applications can be formulated as optimization constrained by conservation laws. Such optimization can be efficiently solved by gradient-based methods, where the gradient is obtained through the adjoint method. Traditionally, the adjoint method has not been able to be implemented in "gray-box" conservation law simulations. In gray-box simulations, the analytical and numerical form of the conservation law is unknown, but the space-time solution of relevant flow quantities is available. Without the adjoint gradient, optimization can be challenging for problems with many control variables. However, much information about the gray-box simulation is contained in its space-time solution, which motivates us to estimate the adjoint gradient by leveraging the space-time solution. This article considers a type of gray-box simulations where the flux function is partially unknown. A method is introduced to estimate the adjoint gradient at a cost independent of the number of control variables. The method firstly infers a conservation law, named the twin model, from the space-time solution, and then applies the adjoint method to the inferred twin model to estimate the gradient. The method is demonstrated to achieve good gradient estimation accuracies in several numerical examples. The main contributions of this paper are: a twin model method that enables the adjoint gradient computation for gray-box conservation law simulations; and an adaptive basis construction scheme that fully exploits the information of gray-box solutions.

---

## Notations

- $t \in [0, T]$ : the time,
- $\{t_i\}_{i=1}^M$ : the time discretization,
- $x \in \Omega$ : the space,
- $\{x_j\}_{j=1}^N$ : the space discretization,
- $u$ : the space-time solution of gray-box conservation law,
- $\tilde{u}$ : the space-time solution of twin-model conservation law,
- $\mathbf{u}$ : the discretized space-time solution of gray-box simulator,
- $\tilde{\mathbf{u}}$ : the discretized space-time solution of twin-model simulator,
- $k$ : 1) the number of equations of the conservation law; or 2) the number of folds in cross validation.
- $D$ : a differential operator,
- $F$ : the unknown function of the gray-box model,
- $\hat{F}$ : the inferred  $F$ ,
- $q$ : the source term,
- $c$ : the control variables,

<sup>†</sup> Aerospace Computational Design Laboratory, Massachusetts Institute of Technology

- $w$ : the quadrature weights in the numerical space-time integration,
- $\xi$ : the objective function,
- $c_{\min}, c_{\max}$ : bound constraints,
- $d$ : the number of control variables,
- $\mathcal{C} \subset \mathbb{R}^d$ : the control space,
- $\mathcal{M}$ : the solution mismatch,
- $\overline{\mathcal{M}}$ : the mean solution mismatch in cross validation,
- $\phi$ : the basis functions for  $\tilde{F}$ ,
- $\alpha$ : the coefficients for  $\phi$ ,
- $\mathcal{A}$ : the index set for a basis dictionary,
- $T$ : twin model,
- $\tau$ : residual,
- $\boldsymbol{\tau}$ : discretized residual,
- $\mathcal{T}$ : integrated truncation error.

## 1. Motivation

A conservation law states that a particular property of a physical system does not appear or vanish as the system evolves over time, such as the conservation of mass, momentum, and energy. Mathematically, a conservation law can be expressed locally as a continuity equation (1.1),

$$\frac{\partial u}{\partial t} + \nabla \cdot F = q, \quad (1.1)$$

where  $u$  is the conserved physical quantity,  $t$  is time,  $F$  is the flux of  $u$ , and  $q$  is the source for  $u$ . Many equations fundamental to the physical world, such as the Navier-Stokes equation, the Maxwell equation, and the porous medium transport equation, can be described by (1.1).

Optimization constrained by conservation laws is present in many engineering applications. For example, in gas turbines, the rotor blades can operate at a temperature close to 2000K Han (12). To prevent material failure due to overheating, channels can be drilled inside the rotor blades to circulate coolant air whose dynamics are governed by the Navier-Stokes equation Verstraete (13). The pressure used to drive the coolant flow is provided by the compressor, resulting in a penalty on the turbine’s thermo-dynamic efficiency Coletti (13). Engineers are thereby interested in optimizing the coolant channel geometry in order to suppress the pressure loss. In this optimization problem, the control variables are the parameters that describe the channel geometry. The dimensionality of the optimization is the number of control variables, i.e. the control’s degree of freedom. Another example is the field control of petroleum reservoir. In petroleum reservoir, the fluid flow of various phases and chemical components is dictated by porous medium transport equations Peaceman (00). The flow can be passively and actively controlled by a variety of techniques Ramirez (87), such as the wellbore pressure control, the polymer injection, and the steam heating, where the reservoir is controlled by the pressure at each wells, by the the injection rate of polymer, and by the temperature of the steam Alvarado (10). The pressure, injection rate, and temperature can vary in each well and at every day over decades of continuous operations. The dimensionality of the optimization is the total number of these control variables. Driven by economic interests, petroleum

producers are devoted to optimizing the controls for enhanced recovery and reduced cost.

Such optimization is being revolutionized by the numerical simulation and optimization algorithms. On one hand, conservation law simulation can provide an evaluation of a candidate control that is cheaper, faster, and more scalable than conducting physical experiments. On the other hand, advanced optimization algorithms can guide the control towards the optimal with reduced number of simulation Dennis (77); Rios (13); Nocedal (80); Conn (09); Holland (75); Banks (07); Yang (10); Mokus (78). However, optimization based on conservation law simulation can still be overwhelmingly costly. The cost is two-folded: Firstly, each simulation for a given control may run for hours or days even on a high-end computer. This is mainly because of the high-fidelity physical models, the complex numerical schemes, and the large scale space-time discretization employed in the simulation. Secondly, optimization algorithms generally take many iterations of simulation on various controls. The number of iterations required to achieve near-optimality usually increases with the control's degree of freedom Fu (94). The two costs are multiplicative. The multiplicative effect compromises the impact of computational efforts among field engineers.

Fortunately, the cost due to iteration can be alleviated by adopting gradient-based optimization algorithms Fu (94). A gradient-based algorithm usually requires significantly less iterations than a derivative-free algorithm for problems with many control variables Giles (00); Fu (94); Rios (13). Gradient-based algorithms require the gradient of the optimization objective to the control variables, which is efficiently computable through the adjoint method Lions (71). The adjoint method propagates the gradient from the objective backward to the control variables through the path of time integration Lions (71) or through the chain of numerical operations Corliss (02). To keep track of the back propagation, the simulator source code needs to be available. In real-world industrial simulators, adjoint is scarcely implemented because most source codes are proprietary and/or legacy. For example, *PSim*, a reservoir simulator developed and owned by *ConocoPhillips*, is a multi-million-line Fortran-77 code that traces its birth back to the 1980's. Implementing adjoint directly into the source code is unpreferable because it can take tremendous amount of brain hours. Besides, the source code and its physical models are only accessible and modifiable by the computational team inside the company. For the sake of gradient computation, *PSim* has been superseded by adjoint-enabled simulators, but it is difficult to be replaced due to its legacy use and cost concerns. The proprietary and legacy nature of many industrial simulators hinders the prevalence of the adjoint method and gradient-based algorithms in many real-world problems with high-dimensional control.

Despite their proprietary and legacy nature, most simulators for unsteady conservation laws are able to provide the discretized space-time solution of relevant flow quantities. For example, *PSim* provides the space-time solution of pressure, saturation, and concentration for multi-phase flow. Similarly, most steady state simulators are able to provide the spatial solution. the discussion will focus on the unsteady case, since a steady state simulator can be viewed as a special case of the unsteady one where the solution remains the same over many time steps.

I argue that the adjoint gradient computation may be enabled by leveraging the space-

time solution. The discretized space-time solution provides invaluable information about the conservation law hardwired in the simulator. For illustration, consider a code which simulates

$$\frac{\partial u}{\partial t} + \frac{\partial F(u)}{\partial x} = c, \quad x \in [0, 1], \quad t \in [0, 1] \quad (1.2)$$

with proper initial and boundary conditions and  $F$  being differentiable.  $c$  indicates the control that acts as a source for  $u$ . If the expression of  $F(u)$  in the simulator is not accessible by the user, adjoint can not be implemented directly. However,  $F$  may be partially inferred from a discretized space-time solution of  $u$  for a given  $c$ . To see this, let the discretized solution be  $\mathbf{u} \equiv \{u(t_i, x_j)\}_{i=1, \dots, M, j=1, \dots, N}$ , where  $0 \leq t_1 < t_2 < \dots < t_M \leq 1$  and  $0 \leq x_1 < x_2 < \dots < x_N \leq 1$  indicate the time and space discretization. Given  $\mathbf{u}$ , the  $\frac{\partial u}{\partial t}$  and  $\frac{\partial u}{\partial x}$  can be sampled by finite difference. Because (1.2) can be written as

$$\frac{\partial u}{\partial t} + \frac{dF}{du} \frac{\partial u}{\partial x} = c, \quad x \in [0, 1], \quad t \in [0, 1] \quad (1.3)$$

away from the shock wave, the samples of  $\frac{\partial u}{\partial t}$  and  $\frac{\partial u}{\partial x}$  can be plugged into (1.3) to obtain samples of  $\frac{dF}{du}$ . The reasoning remains intact at the shock wave, where  $\frac{dF}{du}$  in (1.3) is replaced by the finite difference form  $\frac{\Delta F}{\Delta u}$  according to the Rankine-Hugoniot condition. Based upon the sampled  $\frac{dF}{du}$  and  $\frac{\Delta F}{\Delta u}$ , the unknown flux function  $F$  can be approximated up to a constant for values of  $u$  that appeared in the solution, by using indefinite integral. Let  $\tilde{F}$  be the approximation for  $F$ . An alternative conservation law can be proposed

$$\frac{\partial \tilde{u}}{\partial t} + \frac{\partial \tilde{F}(\tilde{u})}{\partial \tilde{u}} = c, \quad x \in [0, 1], \quad t \in [0, 1], \quad (1.4)$$

that approximates the true but unknown conservation law (1.2), where  $\tilde{u}$  is the solution associated with  $\tilde{F}$ , in the following sense: If  $\tilde{F}$  and  $F$  are off by a constant  $a$ , i.e.  $\tilde{F} = F + a$ , then  $\frac{\partial F(u)}{\partial u} = \frac{\partial(F(u)+a)}{\partial u} = \frac{\partial \tilde{F}(u)}{\partial u}$ ; therefore, the solutions of (1.2) and (1.4) to any initial value problem will be the same. In addition, the solutions to any adjoint equation, with any objective function, will be the same. As a result, the gradient computed by the adjoint equation of (1.4) will be the true gradient, and therefore can drive the optimization constrained by (1.2). A simulator for the approximated conservation law is named **twin model**, since it behaves as an adjoint-enabled twin of the original simulator. If a conservation law has a system of equations and/or has a greater-than-one spatial dimension, the above simple method to recover the flux function from a solution will no longer work. Nonetheless, much information about the flux function can be extracted from the solution. Given some additional information of the conservation law, one may be able to recover the unknown aspects of the flux function. The details of this topic are discussed in Section 4.

This article focuses on a class of simulators that I call **gray-box**. A simulator is defined to be gray-box if the following two conditions are met:

- (a) the adjoint is unavailable, and is impractical to implement into the source code.
- (b) the full space-time solution of relevant flow quantities is available.

Many industrial simulators, such as *PSim*, satisfy both conditions. In contrast, a simulator is named **open-box** if condition 1 is violated. For example, *OpenFOAM* OpenFOAM (16) is an open-source fluid simulator where adjoint can be implemented directly into its source code, so it is open-box by definition. Open-box simulators enjoy the benefit of

efficient gradient computation brought by adjoint, thereby are not within the research scope of the article. If condition 1 is met but 2 is violated, a simulator is named **black-box**. For example, *Aspen Aspen* (16), an industrial chemical reactor simulator, provides neither the adjoint nor the full space-time solution. Black-box simulators are simply calculators for the objective function. Due to the lack of space-time solution, adjoint can not be enabled using the twin model. Gray-box simulators are ubiquitous in many engineering applications. Examples are *Fluent FLUENT* (11) and *CFX CFX* (12) for computational fluid dynamics, and *ECLIPSE* (Schlumberger), *PSim* (ConocoPhillips), and *MORES* (Shell) for petroleum reservoir simulations. This article will only investigate gray-box simulators.

This article aims at estimating the adjoint gradient at a cost independent of the number of control variables. Motivated by the adjoint gradient computation, a mathematical procedure for the estimation is developed by using the full space-time solution. In a companion paper, I examine how the estimated gradient can facilitate a suitable optimization algorithm to reduce the number of iterations.

Instead of discussing gray-box simulators in general, this article only focuses on simulators with partially unknown flux function, while their boundary condition, initial condition, and the source term are known. For example, one may know that the flux depends on certain variables, but the specific function form of such dependence is unknown. This assumption is valid for some applications, such as simulating a petroleum reservoir with polymer injection. The flow in such reservoir is governed by multi-phase multi-component porous medium transport equations Peaceman (00). The initial condition is usually given at the equilibrium state, the boundary is usually described by a no-flux condition, and the source term can be modeled as controls with given flow rate or wellbore pressure. Usually the flux function is given by the Darcy's law. The Darcy's law involves physical models like the permeability<sup>†</sup> and the viscosity<sup>‡</sup>. The mechanism through which the injected polymer modifies the rock permeability and flow viscosity can be unavailable. Thereby the flux is partially unknown. The specific form of PDE considered in this article is given in Section 2. It is a future work to extend my research to more general gray-box settings where the initial condition, boundary condition, source term, and the flux are jointly unknown.

## 2. Problem Formulation

Consider an objective function

$$\xi(\mathbf{u}, c) = \sum_{i=1}^M \sum_{j=1}^N w_{ij} f(\mathbf{u}_{ij}, c; t_i, x_j) \approx \int_0^T \int_{\Omega} f(u, c; t, x) dx dt \quad (2.1)$$

where  $\mathbf{u}$  is the discretized space-time solution of a gray-box conservation law simulator. The spatial coordinate is  $x \in \Omega$  and the time is  $t \in [0, T]$ .  $i = 1, \dots, M$  and  $j = 1, \dots, N$  indicate the indices for the time and space discretization.  $f$  is a given function that depends on  $u$ ,  $c$ ,  $t$ , and  $x$ .  $w_{ij}$ 's are given quadrature weights for the integration.  $c \in \mathbb{R}^d$

<sup>†</sup> The permeability quantifies the easiness of liquids to pass through the rock.

<sup>‡</sup> The viscosity quantifies the internal friction of the liquid flow.

indicates the control variable.

The gray-box simulator solves the partial differential equation (PDE)

$$\frac{\partial u}{\partial t} + \nabla \cdot (DF(u)) = q(u, c), \quad (2.2)$$

which is a system of  $k$  equation. The initial and boundary conditions are known.  $D$  is a known differential operator that may depend on  $u$ , and  $F$  is an unknown function that depends on  $u$ .  $q$  is a known source term that depends on  $u$  and  $c$ . Notice (2.2) degenerates to (1.1) when  $D$  equals 1. The simulator does not have the adjoint capability, and it is infeasible to implement the adjoint method into its source code. But the full space-time solution  $\mathbf{u}$  is provided. The steady-state conservation law is a special case of the unsteady one, so it will not be discussed separately.

### 3. Literature Review

Given the background, I review the literature on derivative-free optimization and gradient-based optimization. In addition, I review the adjoint method. Finally, I review methods for adaptive basis construction, which is useful for the adaptive parameterization of a twin model.

#### 3.1. Review of Optimization Methods

Optimization methods can be categorized into derivative-free and gradient-based methods Rios (13), depending on whether the gradient information is used. In the sequel, I review the two types of methods.

##### 3.1.1. Derivative-free Optimization

Derivative-free optimization (DFO) requires only the availability of objective function values but no gradient information Rios (13), thus is useful when the gradient is unavailable, unreliable, or too expensive to obtain. Such methods are suitable for problems constrained by black-box simulators.

Depending on whether a local or global optimum is desired, DFO methods can be categorized into local methods and global methods Rios (13). Local methods seek a local optimum which is also the global optimum for convex problems. An important local method is the trust-region method Conn (00). Trust-region method introduces a surrogate model that is cheap to evaluate and presumably accurate within a trust region: an adaptive neighborhood around the current iterate Conn (00). At each iteration, the surrogate is optimized in a domain bounded by the trust region to generate candidate steps for additional objective evaluations Conn (00). The surrogates can be constructed either by interpolating the objective evaluations Powell (94); Wild (13), or by running a low-fidelity simulation Alexandrov (01, 98). Convergence to the objective function's optimum is guaranteed by ensuring that the surrogate have the same value and gradient as the objective function when the size of the trust region shrinks to zero Conn (09); Wild (13).

Global methods seek the global optimum. Example methods include the branch-and-bound search Pint (96), evolution methods Schwefel (93), and Bayesian methods Snoek

(12); Locatelli (97); Kushner (64). The branch-and-bound search sequentially partitions the entire control space into a tree structure, and determines lower and upper bounds for the optimum Pint (96). Partitions that are inferior are eliminated in the course of the search Pint (96). The bounds are usually obtained through the assumption of the Lipschitz continuity or statistical bounds for the objective function Pint (96). Evolution methods maintain a population of candidate controls, which adapts and mutates in a way that resembles natural phenomena such as the natural selection Holland (75); Yang (10) and the swarm intelligence Banks (07). Bayesian methods model the objective function as a random member function from a stochastic process. At each iteration, the statistics of the stochastic process are calculated and the posterior, a probability measure, of the objective is updated using Bayesian metrics Snoek (12); Mokus (78). The posterior is used to pick the next candidate step that best balances the exploration of unsampled regions and the exploitation around the sampled optimum Locatelli (97); Jones (98); Srinivas (09).

Because many real-world problems are non-convex, global methods are usually preferred to local methods if the global optimum is desired Rios (13). Besides, DFO methods usually require a large number of function evaluations to converge, especially when the dimension of control is large Rios (13). This issue can be alleviated by incorporating the gradient information Zhou (08); Chung (01); Noel (12); Yang (14). The details are discussed in the next subsection.

### 3.1.2. Gradient-based Optimization

Gradient-based optimization (GBO) requires the availability of the gradient values Fu (94); Bertsekas (99). A gradient value, if exists, provides the optimal infinitesimal change of control variables at each iterate, thus is useful in searching for a better control. Similar to DFO, GBO can also be categorized into local methods and global methods Fu (94). Examples of local GBO methods include the gradient descent methods Spall (05); Armijo (66), the conjugate gradient methods Fletcher (64); Dai (99), and the quasi-Newton methods Dennis (77); Nocedal (80). The gradient descent methods and the conjugate gradient methods choose the search step in the direction of either the gradient Spall (05); Armijo (66) or a conjugate gradient Fletcher (64); Dai (99). Quasi-Newton methods, such as the Broyden-Fletcher-Goldfarb-Shannon (BFGS) method Dennis (77), approximate the Hessian matrix using a series of gradient values. The approximated Hessian allows a local quadratic approximation to the objective function which determines the search direction and stepsize by the Newton's method Dennis (77). In addition, some local DFO methods can be enhanced to use gradient information Carter (91, 93). For instance, in trust-region methods, the construction of local surrogates can incorporate gradient values if available Carter (91, 93). The usage of gradient usually improves the surrogate's accuracy thus enhances the quality of the search step, thereby reducing the required number of iterations Carter (91, 93).

Global GBO methods search for the global optimum using gradient values Fu (94); Bertsekas (99). Many global GBO methods can trace their development to corresponding DFO methods Gudmundsson (98); Zilinskas (08); Noel (12); Yang (14); Chung (01). For example, the stochastic gradient-based global optimization method (StoGo) Gudmundsson (98); Zilinskas (08) works by partitioning the control space and bounding the optimum in the same way as the branch-and-bound method Pint (96). But the

search in each partition is performed by gradient-based algorithms such as BFGS Dennis (77). Similarly, some gradient-based evolution methods, such as the gradient-based particle swarm method Noel (12) and the gradient-based cuckoo search method Yang (14), can be viewed as gradient variations of corresponding derivative-free counterparts Banks (07); Yang (10). For example, the gradient-based particle swarm method combines particle swarm algorithm with the stochastic gradient descent method Noel (12). The movement of each particle is dictated not only by the function evaluations of all particles, but also by its local gradient Noel (12).

To achieve a desired objective value, GBO methods generally require much less iterations than DFO methods for problems with many control variables Fu (94); Bertsekas (99). GBO methods can be efficiently applied to optimization constrained by open-box simulators, because the gradient is efficiently computable by the adjoint method Lions (71); Fu (94). In a companion paper, I extend GBO to optimization constrained by gray-box simulation by estimating the gradient using the full space-time solution.

### 3.2. The Adjoint Method

Consider a differentiable objective function constrained by a conservation law PDE (2.2). Let the objective function be  $\xi(u, c)$ ,  $c \in \mathbb{R}^d$ , and let the PDE (2.2) be abstracted as  $\mathcal{F}(u, c) = 0$ .  $\mathcal{F}$  is a parameterized differential operator, together with boundary conditions and/or initial conditions, that uniquely defines a  $u$  for each  $c$ . The gradient  $\frac{d\xi}{dc}$  can be estimated trivially by finite difference. The  $i$ th component of the gradient is given by

$$\left(\frac{d\xi}{dc}\right)_i \approx \frac{1}{\delta}(\xi(u + \Delta u_i, c + \delta e_i) - \xi(u, c)), \quad (3.1)$$

where

$$\mathcal{F}(u, c) = 0, \quad \mathcal{F}(u + \Delta u_i, c + \delta e_i) = 0. \quad (3.2)$$

$e_i$  indicates the  $i$ th unit Cartesian basis vector in  $\mathbb{R}^d$ , and  $\delta > 0$  indicates a small perturbation. Because (3.2) needs to be solved for every  $\delta e_i$ , so that the corresponding  $\Delta u_i$  can be used in (3.1),  $d + 1$  PDE simulations are required to evaluate the gradient. As explained in Section 3.1,  $d$  can be large in many control optimization problems. Therefore, it can be costly to evaluate the gradient by finite difference.

In contrast, the adjoint method evaluates the gradient using only one PDE simulation plus one adjoint simulation Lions (71). To see this, linearize  $\mathcal{F}(u, c) = 0$  into a variational form

$$\delta\mathcal{F} = \frac{\partial\mathcal{F}}{\partial u}\delta u + \frac{\partial\mathcal{F}}{\partial c}\delta c = 0, \quad (3.3)$$

which gives

$$\frac{du}{dc} = -\left(\frac{\partial\mathcal{F}}{\partial u}\right)^{-1}\frac{\partial\mathcal{F}}{\partial c} \quad (3.4)$$



Using (3.4),  $\frac{d\xi}{dc}$  can be expressed by

$$\begin{aligned}\frac{d\xi}{dc} &= \frac{\partial\xi}{\partial u} \frac{du}{dc} + \frac{\partial\xi}{\partial c} \\ &= -\frac{\partial\xi}{\partial u} \left( \frac{\partial\mathcal{F}}{\partial u} \right)^{-1} \frac{\partial\mathcal{F}}{\partial c} + \frac{\partial\xi}{\partial c}, \\ &= -\lambda^T \frac{\partial\mathcal{F}}{\partial c} + \frac{\partial\xi}{\partial c}\end{aligned}\quad (3.5)$$

where  $\lambda$ , the adjoint state, is given by the adjoint equation

$$\left( \frac{\partial\mathcal{F}}{\partial u} \right)^T \lambda = \left( \frac{\partial\xi}{\partial u} \right)^T \quad (3.6)$$

Therefore, the gradient can be evaluated by (3.5) using one simulation of  $\mathcal{F}(u, c) = 0$  and one simulation of (3.6) that solves for  $\lambda$ .

Adjoint methods can be categorized into continuous adjoint and discrete adjoint methods, depending on whether the linearization or the discretization is executed first Plessix (06). The above procedure, (3.3) thru. (3.6), is the continuous adjoint, where  $\mathcal{F}$  is a differential operator. The continuous adjoint method linearizes the continuous PDE  $\mathcal{F}(u, c) = 0$  first, then discretizes the adjoint equation (3.6) Lions (71). In (3.6),  $\left( \frac{\partial\mathcal{F}}{\partial u} \right)^T$  can be derived as another differential operator. With proper boundary and/or initial conditions, it uniquely determines the adjoint solution  $\lambda$ . See Giles (00) for a detailed derivation of the continuous adjoint equation.

The discrete adjoint method Giles (03) discretizes  $\mathcal{F}(u, c) = 0$  first. After the discretization,  $u$  and  $c$  become vectors  $\mathbf{u}$  and  $\mathbf{c}$ .  $\mathbf{u}$  is defined implicitly by the system  $\mathcal{F}_d(\mathbf{u}, \mathbf{c}) = 0$ , where  $\mathcal{F}_d$  indicates the discretized difference operator. Using the same derivation as (3.3) thru. (3.6), the discrete adjoint equation can be obtained

$$\left( \frac{\partial\mathcal{F}_d}{\partial\mathbf{u}} \right)^T \boldsymbol{\lambda} = \left( \frac{\partial\xi}{\partial\mathbf{u}} \right)^T, \quad (3.7)$$

which is a linear system of equations.  $\left( \frac{\partial\mathcal{F}_d}{\partial\mathbf{u}} \right)^T$  is derived as another difference operator. With proper discretized boundary/initial conditions, it uniquely determines the discrete adjoint vector  $\boldsymbol{\lambda}$ , which subsequently determines the gradient

$$\frac{d\xi}{d\mathbf{c}} = -\boldsymbol{\lambda}^T \frac{\partial\mathcal{F}_d}{\partial\mathbf{c}} + \frac{\partial\xi}{\partial\mathbf{c}}. \quad (3.8)$$

See Chapter 1 of Schneider (06) for a detailed derivation of the discrete adjoint.

The discrete adjoint method can be implemented by automatic differentiation (AD) Corliss (02). AD exploits the fact that a PDE simulation, no matter how complicated, executes a sequence of elementary arithmetic operations (e.g. addition, multiplication) and elementary functions (e.g. exp, sin) Corliss (02). For example, consider the function

$$\xi = f(c_1, c_2) = c_1 c_2 + \sin(c_1). \quad (3.9)$$

The function can be broken down into a series of elementary arithmetic operations and

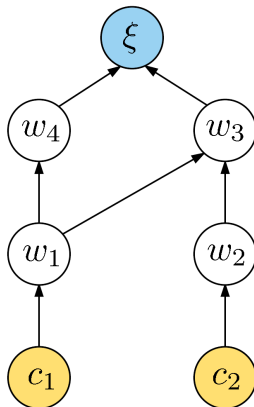


Figure 1: The computational graph for (3.10). The yellow nodes indicate the input variables, the blue node indicates the output variable, and the white nodes indicate the intermediate variables. The arrows indicate elementary operations. The beginning and end nodes of each arrow indicate the independent and dependent variables for each operation.

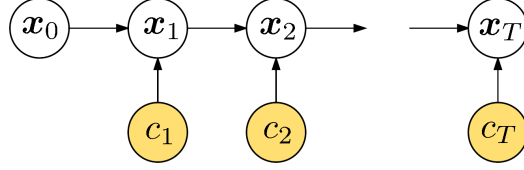
elementary functions.

$$\begin{aligned}
 w_1 &= c_1 \\
 w_2 &= c_2 \\
 w_3 &= w_1 w_2 \\
 w_4 &= \sin(w_1) \\
 \xi &= w_3 + w_4 .
 \end{aligned} \tag{3.10}$$

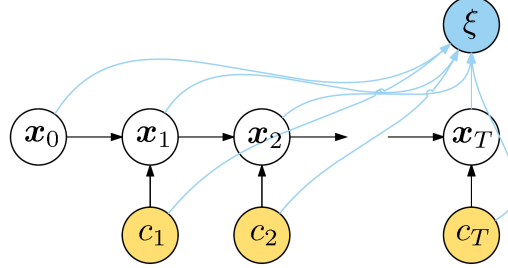
(3.10) can be represented by a computational graph in Figure 1. In the graph, the gradient of the output with respect to the input variables can be computed using the chain rule Corliss (02). Let  $\bar{z}$  denote the gradient of  $\xi$  with respect to  $z$ , for any independent or intermediate variable  $z$  in (3.10). To compute the derivatives  $\bar{c}_1 = \frac{\partial \xi}{\partial c_1}$  and  $\bar{c}_2 = \frac{\partial \xi}{\partial c_2}$ , one can propagate the derivatives backward in the computational graph as follows

$$\begin{aligned}
 \bar{w}_4 &= 1 \\
 \bar{w}_3 &= 1 \\
 \bar{w}_2 &= \bar{w}_3 \frac{\partial w_3}{\partial w_2} = 1 \cdot w_1 \\
 \bar{w}_1 &= \bar{w}_4 \frac{\partial w_4}{\partial w_1} + \bar{w}_3 \frac{\partial w_3}{\partial w_1} = 1 \cdot \cos(w_1) + 1 \cdot w_2 \\
 \bar{c}_2 &= \bar{w}_2 = c_1 \\
 \bar{c}_1 &= \bar{w}_1 = \cos(c_1) + c_2
 \end{aligned} \tag{3.11}$$

The derivatives in (3.11) are straightforward to compute. This is because every forward operation in (3.10) is elementary, and their derivatives can be hardwired in AD softwares. Notice each arrow in Figure 1 is traversed once and only once in the backward propagation (3.11). Therefore, the backward gradient computation has a similar cost as the forward output computation, regardless of the number of input variables. See Corliss



(a) The computational graph for (3.12), which is constructed by (3.13). The yellow nodes indicate the input variables.



(b) The computational graph for evaluating the objective function  $\xi$ . The blue node indicates the output variable.

Figure 2: Computational graphs for the PDE simulation and objective evaluation.

(02) for a thorough review of AD.

Because a PDE simulation can be viewed as performing a sequence of elementary operations, AD can be used to evaluate the discrete adjoint. Consider a discretized PDE simulation that at each timestep solves

$$\mathcal{F}_{t+1} = \mathcal{F}(\mathbf{x}_t, \mathbf{x}_{t+1}, \mathbf{c}_{t+1}) = 0, \quad (3.12)$$

for  $t = 0, \dots, T-1$ , where  $\mathbf{x}_t$  and  $\mathbf{c}_t$  are the state and control variables at the  $t$ th timestep. AD can be used to compute the gradient of an objective function

$$\xi = \xi(\mathbf{x}_0, \dots, \mathbf{x}_T; \mathbf{c}_1, \dots, \mathbf{c}_T)$$

to the control variables. To see this, consider the evaluation of (3.12) using an AD software. The gradients  $\frac{\partial \mathcal{F}_{t+1}}{\partial \mathbf{x}_t}$ ,  $\frac{\partial \mathcal{F}_{t+1}}{\partial \mathbf{x}_{t+1}}$ , and  $\frac{\partial \mathcal{F}_{t+1}}{\partial \mathbf{c}_{t+1}}$ , for  $t = 0, \dots, T-1$ , are automatically computable. Therefore, one can obtain

$$\begin{aligned} \frac{\partial \mathbf{x}_{t+1}}{\partial \mathbf{x}_t} &= - \left( \frac{\partial \mathcal{F}_{t+1}}{\partial \mathbf{x}_{t+1}} \right)^{-1} \left( \frac{\partial \mathcal{F}_{t+1}}{\partial \mathbf{x}_t} \right) \\ \frac{\partial \mathbf{x}_{t+1}}{\partial \mathbf{c}_{t+1}} &= - \left( \frac{\partial \mathcal{F}_{t+1}}{\partial \mathbf{x}_{t+1}} \right)^{-1} \left( \frac{\partial \mathcal{F}_{t+1}}{\partial \mathbf{c}_{t+1}} \right). \end{aligned} \quad (3.13)$$

Therefore a computational graph, Figure 2a, can be constructed using the chain rule. The graph enables the evaluation of all  $\frac{\partial \mathbf{x}_t}{\partial \mathbf{c}_{t-i}}$ , for  $t = 1, \dots, T$  and  $i = 0, \dots, t-1$ . Given the solutions  $\mathbf{x}_t$ 's and the controls  $\mathbf{c}_t$ 's, the evaluation of  $\xi$  is nothing but overlaying the graph by an additional layer of computations, shown in Figure 2b. Because  $\frac{\partial \xi}{\partial \mathbf{x}_t}$ 's and

$\frac{\partial \xi}{\partial \mathbf{c}_t}$ 's can be obtained by AD, the gradient

$$\frac{d\xi}{d\mathbf{c}_t} = \frac{\partial \xi}{\partial \mathbf{c}_t} + \frac{\partial \xi}{\partial \mathbf{x}_t} \frac{\partial \mathbf{x}_t}{\partial \mathbf{c}_t} + \frac{\partial \xi}{\partial \mathbf{x}_{t+1}} \frac{\partial \mathbf{x}_{t+1}}{\partial \mathbf{c}_t} + \dots + \frac{\partial \xi}{\partial \mathbf{x}_T} \frac{\partial \mathbf{x}_T}{\partial \mathbf{c}_t} \quad (3.14)$$

can be computed, for all  $t = 1, \dots, T$ .

The adjoint method has seen wide applications in optimization problems constrained by conservation law simulations, such as in airfoil design Jameson (88); Anderson (99); Renaud (97), adaptive mesh refinement Schneider (06), injection policy optimization in petroleum reservoirs Ramirez (84), history matching in reservoir geophysics Plessix (06), and optimal well placement in reservoir management Zandvliet (08). Besides, there are many free AD softwares available for various languages, such as *ADOL-C* (C, C++) Walther (12), *Adiff* (Matlab) Mcilhagga (13), and *Theano* (Python) Bergstra (10). Unfortunately, the adjoint method is not directly applicable to gray-box simulations, as explained in Section 1. To break this limitation, section 4 develops the twin model method that enables the adjoint gradient computation for gray-box simulations.

### 3.3. Adaptive Basis Construction

The unknown function  $F$  in (2.2) can be approximated by a linear combination of basis functions. An over-complete or incomplete set of bases can negatively affect the approximation due to overfitting or underfitting. Therefore, adaptive basis construction is needed.

Square-integrable functions can be represented by the parameterization<sup>†</sup> Taylor (58)

$$\tilde{F}(\cdot) = \sum_{i \in \mathbb{N}} \alpha_i \phi_i(\cdot), \quad (3.15)$$

where  $\phi_i$ 's are linearly-independent basis functions,  $\alpha_i$ 's are the coefficients, and  $i$  indices the basis. For example, a bivariate function can be represented by monomials (Weierstrass approximation theorem Taylor (58))

$$1, u_1, u_1^2, u_2, u_1 u_2, u_1^2 u_2, u_2^2, u_1 u_2^2, u_1^2 u_2^2, \dots$$

on any real interval  $[a, b]$ .

Let  $\mathcal{A}$  be a non-empty finite subset of  $\mathbb{N}$ ,  $\tilde{F}$  can be approximated using a subset of bases,

$$\tilde{F}(\cdot) \approx \sum_{i \in \mathcal{A}} \alpha_i \phi_i(\cdot), \quad (3.16)$$

where  $\{\phi_i\}_{i \in \mathcal{A}}$  is called a basis dictionary Mallat (93). The approximation is solely determined by the choices of the dictionary and the coefficients. For example, in polynomial

<sup>†</sup> By definition, the square integrable functions form a pre-Hilbert space with inner product given by  $\langle f, g \rangle = \int_A f(x)g(x)dx$ , where 1)  $f$  and  $g$  are square integrable functions, 2)  $f(x)$  is the complex conjugate of  $f(x)$ , and 3)  $A$  is the set over which the integral is defined. It can be shown that square integrable functions are complete under the metric induced by the inner product, thus is a Hilbert space Taylor (58). Any member function can be represented by a finite or countably infinite number of basis functions of the Hilbert space Taylor (58).

approximation, the basis dictionary can consist of the basis whose total polynomial degree does not exceed  $p \in \mathbb{N}$  Ghanem (03). Given a dictionary, the coefficients for  $\tilde{F}$  can be determined by the minimization Ghanem (03)

$$\boldsymbol{\alpha}^* = \operatorname{argmin}_{\boldsymbol{\alpha} \in \mathbb{R}^{|\mathcal{A}|}} \left\| \tilde{F} - \sum_{i \in \mathcal{A}} \alpha_i \phi_i \right\|_{L_p}, \quad (3.17)$$

where  $\|\cdot\|_{L_p}$  indicates the  $L_p$  norm<sup>†</sup>. This article parameterizes the twin-model flux  $\tilde{F}$  and optimizes the coefficients, so the twin model serves as a proxy of the gray-box model. Details are discussed in Section 4.2.

If the dictionary is pre-determined without using any evaluation of the underlying function, its cardinality can increase as the number of variables increases, and as the basis complexity increases Ghanem (03). For example, for  $d$ -variate polynomial basis, the total number of bases is  $d^p$  if one bounds the polynomial degree of each variable by  $p$ ; and is  $\binom{p+d}{d}$  if one bounds the total degree by  $p$  Ghanem (03). For piecewise linear basis, one can approximate the function using Smolyak’s sparse grid with  $\mathcal{O}(n(\log n)^{d-1})$  bases<sup>‡</sup>, where  $n$  is the number of univariate basis for each variable.

In many applications, one may deliver a similarly accurate approximation by using a much smaller subset of the dictionary as the bases than using the full dictionary Ghanem (03); Chen (01); Mallat (93); Tibshirani (96). To exploit the sparse structure, only significant bases shall be selected, and the selection process shall be adaptive depending on the values of function evaluations. There are several methods that adaptively determine the sparsity, such as Lasso regularization Tibshirani (96), matching pursuit Mallat (93), and basis pursuit Chen (01). Lasso regularization adds a penalty  $\lambda \sum_{i \in \mathcal{A}} |\alpha_i|$  to the approximation error, where  $\lambda > 0$  is a tunable parameter Tibshirani (96). In this way, Lasso balances the approximation error and the number of non-zero coefficients Tibshirani (96). Matching pursuit adopts a greedy, stepwise approach Mallat (93). It either selects a significant basis one-at-a-time (forward selection) from a dictionary Friedman (94), or prunes an insignificant basis one-at-a-time (backward pruning) from the dictionary Reed (93). Basis pursuit minimizes  $\|\boldsymbol{\alpha}\|_{L_1}$  subject to (3.15), which is equivalently reformulated and efficiently solved as a linear programming problem Chen (01).

Conventionally, the dictionary for the sparse approximation needs to be pre-determined, with the belief that the dictionary is a superset of the significant bases Blatman (08). This can be problematic because the maximum complexity<sup>¶</sup> of the significant ones are unknown a priori. To address this issue, methods have been devised that construct an adaptive dictionary Jekabsons (10); Blatman (08, 10). Although different in details,

<sup>†</sup> Usually  $p = 1$  Chen (01) or 2 Daubechies (88); Mallat (93).

<sup>‡</sup> To be precise, if the underlying function has bounded mixed second derivatives  $D^{\boldsymbol{\beta}} = \frac{\partial^{|\boldsymbol{\beta}|}}{\partial u_1^{\beta_1} \dots \partial u_d^{\beta_d}}$  for  $|\boldsymbol{\beta}|_{\infty} \leq 2$ , and is defined in a  $d$ -dimensional unit cube, then the error between the underlying function  $\tilde{F}$  and the approximation  $\hat{\tilde{F}}$  is  $\|\tilde{F} - \hat{\tilde{F}}\|_{L_2} = \mathcal{O}(4^{-n} n^{d-1})$  Smolyak (60).

<sup>¶</sup> The definition of complexity is basis-dependent. For example, the complexity for polynomial basis can be its total polynomial degree; and the complexity for wavelet basis can be its finest resolution Mallat (89). Here the “complexity” is discussed in a general sense.

such methods share the same approach: Starting from some trivial bases<sup>||</sup>, a dictionary is built up progressively by iterating over a forward step and a backward step Jekabsons (10); Blatman (08, 10). The forward step searches over a candidate set of bases, and appends the significant ones to the dictionary Jekabsons (10); Blatman (08, 10). The backward step searches over the current dictionary, and removes the insignificant ones from the dictionary Jekabsons (10); Blatman (08, 10). The iteration stops only when no alternation is made to the dictionary or when a targeted accuracy is achieved, without bounding the basis complexity a priori Jekabsons (10); Blatman (08, 10). Such approach is adopted to build up the bases for  $\tilde{F}$ . Details are discussed in Section 4.3.

Based the motivation and literature review, we find a need to enable adjoint gradient computation for gray-box conservation law simulations, especially for problems with many control variables. The objective is to develop an adjoint approach that estimates the gradient of objective functions constrained by gray-box conservation law simulations with partially unknown flux functions, by leveraging the space-time solution. Section 4.1 devises a general framework to estimate the gradient of an objective function constrained by a gray-box simulation, at a cost independent of the gradient’s dimensionality. This is achieved through firstly training a twin model, then applying the adjoint method to the trained twin model. Section 4.2 introduces a parameterization of the unknown flux function, followed by a numerical demonstration that motivates the needs for an adaptive parameterization. Section 4.3 develops an adaptive scheme for the flux function. By summarizing the developments, a twin model algorithm is presented in section 4.4. To reduce the computational cost in training a twin model, a truncation error metric and a pre-train step is developed in section 4.5. Finally, Section 5 demonstrates the twin model algorithm in several numerical examples.

#### 4. Estimate the Gradient by Using the Space-time Solution

This section develops a method to estimate the gradient by using the space-time solution of gray-box conservation law simulations. An example, equation (1.1), has been given in Section 1 to illustrate why such estimation is possible when the conservation law involves only one equation and one dimensional space. In this example, the derivative of the flux can be first interpolated by using the discretized gray-box solution; then the adjoint method is applied to the inferred conservation law (1.4) to estimate the gradient. This section develops a more general procedure suitable for systems of equations and for problems with a spatial dimension greater than one.

##### 4.1. Approach

Consider a gray-box simulator that solves the PDE (2.2), a system of  $k$  equations, for  $u(t, x)$  with  $t \in [0, T]$  and  $x \in \Omega$ . The PDE has an unknown flux  $F$ , but known source term  $q$ , and known initial and boundary conditions. Let its discretized space-time solution be  $\mathbf{u}$ . The article introduces an open-box simulator solving another PDE, namely the twin model,

$$\frac{\partial \tilde{u}}{\partial t} + \nabla \cdot (D\tilde{F}(\tilde{u})) = q(\tilde{u}, c), \quad (4.1)$$

<sup>||</sup> For example, the starting basis can be 1 for polynomial basis Jekabsons (10). The starting bases serve as seeds from which more complex bases grow. See Jekabsons (10); Blatman (08, 10) for more details of the heuristics. The problem will be revisited in Section 4.3 and 4.4.

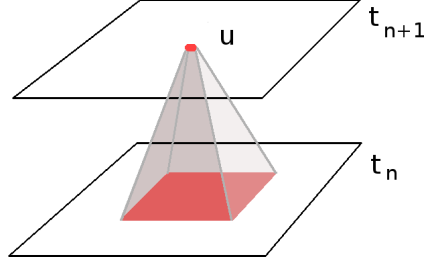


Figure 3: Domain of dependence:  $u(t, x)$  depends on  $u$  at an earlier time within a domain of dependence. The two planes in this figure indicates the spatial solution at two adjacent timesteps. The domain of dependence can be much smaller than  $\Omega$ , the entire spatial domain.

which is a system of  $k$  equations with the same source term and the same initial and boundary conditions. Equation (4.1) differs from (2.2) in its flux. For simplicity, let the open-box simulator use the same space-time discretization, and let its discretized solution be  $\tilde{\mathbf{u}}$ . Define the solution mismatch

$$\mathcal{M}(\tilde{F}) = \sum_{i=1}^M \sum_{j=1}^N w_{ij} (\tilde{\mathbf{u}}_{ij} - \mathbf{u}_{ij})^2, \quad (4.2)$$

where  $w_{ij}$ 's are the quadrature weights for the space-time integration.  $\mathcal{M}$  approximates the space-time integration of the continuous solutions' mismatch,  $\mathcal{M} \approx \int_0^T \int_{\Omega} (\tilde{u}(t, x) - u(t, x))^2 dx dt$ . Given a set  $\mathcal{S}_F$  consisted of all possible guesses for  $F$ , I propose to infer a flux  $\tilde{F}$  such that the mismatch between  $\mathbf{u}$  and  $\tilde{\mathbf{u}}$  is minimized, i.e.

$$\tilde{F}^* = \underset{\tilde{F} \in \mathcal{S}_F}{\operatorname{argmin}} \mathcal{M}, \quad (4.3)$$

The choice for  $\mathcal{S}_F$  will be discussed later in Section 4.2 and 4.3. Because the twin model is open-box, (4.3) can be solved by gradient-based methods. Once  $\mathcal{M}$  is minimized, the adjoint method can be applied to the twin model to estimate the gradient.

The key to inferring the flux is to leverage the gray-box space-time solution. Its inferrability can be loosely explained by the following reasonings. Firstly, the conserved quantity  $u$  in (2.2) depends on  $u$  in a previous time only inside a domain of dependence, illustrated in Figure 3. Similarly, in discretized PDE simulation, the solution at any grid-point only depends on a numerical domain of dependence. Besides, in a PDE simulation, a one-step time marching at any gridpoint can be viewed as a mapping whose input only involves the numerical domain of dependence. Because the number of state variables in the numerical domain of dependence can be small, inference of the mapping is potentially feasible. Secondly, the space-time solution at every space-time gridpoint can be viewed as a sample for this mapping. Because the scale of space-time discretization in a conservation law simulation is usually large, a large number of samples are available for the inference, thus making the inference potentially accurate.

The inferrability is difficult to prove. However, it can be partially justified by the following theorem for PDEs with  $k = 1$  and one dimensional space.

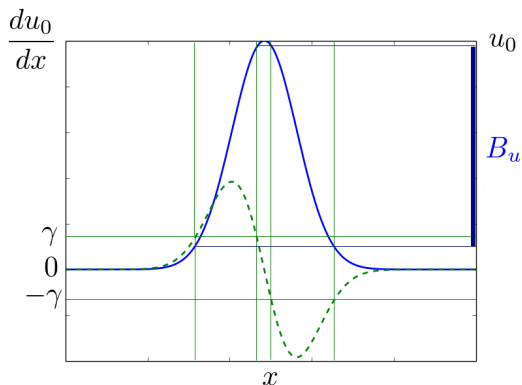


Figure 4: An illustration of  $B_u$  defined in Theorem 1. The blue line is  $u_0$  and the green dashed line is  $\frac{du_0}{dx}$ .  $B_u$  is the set of  $u_0$  where the derivative  $\frac{du_0}{dx}$  has an absolute value larger than  $\gamma$ .

THEOREM 1. Consider two PDEs

$$\frac{\partial u}{\partial t} + \frac{\partial F(u)}{\partial x} = 0, \text{ and} \quad (4.4)$$

$$\frac{\partial \tilde{u}}{\partial t} + \frac{\partial \tilde{F}(\tilde{u})}{\partial x} = 0, \quad (4.5)$$

with the same initial condition  $u(0, x) = u_0(x)$ , and  $x \in \mathbb{R}$ .  $u_0$  is bounded, differentiable, Lipschitz continuous with constant  $L_u$ , and has a finite support.  $F$  and  $\tilde{F}$  are both twice-differentiable and Lipschitz continuous with constant  $L_F$ . Let

$$B_u \equiv \left\{ u \mid u = u_0(x) \text{ that satisfies } \left| \frac{du_0}{dx} \right| \geq \gamma > 0, \text{ for all } x \in \mathbb{R} \right\} \subseteq \mathbb{R}.$$

be a non-empty and measurable set. We have:

For any  $\epsilon > 0$ , there exist  $\delta > 0$  and  $T > 0$  such that

- if  $|\tilde{u}(t, x) - u(t, x)| < \delta$  for any  $x \in \mathbb{R}$  and  $t \in [0, T]$ , then  $\left| \frac{d\tilde{F}}{du} - \frac{dF}{du} \right| < \epsilon$  for any  $u \in B_u$ .

The proof is given in Appendix 7.1. An illustration of  $B_u$  is given in Figure 4. Several observations can be made from Theorem 1. Firstly, if the solutions of (4.4) and (4.5) match closely, then the derivatives of their flux functions must match closely in  $B_u$ . Secondly, the conclusion can only be drawn for  $u \in B_u$  where the initial condition has coverage and has large enough variation. For more general problems involving 1) systems of equations, 2) higher spatial dimensions, and 3) discretization, the inferrability is difficult to show theoretically. Instead, it will be demonstrated numerically.

The next section discusses the choices of  $\mathcal{S}_F$  occurred in (4.3). A suitable parameterization for  $\tilde{F}$  will be chosen that takes into account the observations from Theorem 1.



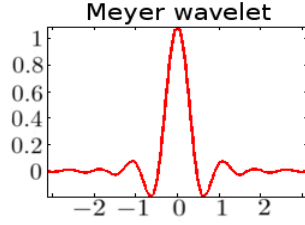


Figure 5: An example of mother wavelet, the Meyer wavelet.

#### 4.2. Parameterization

Functions can be parameterized by a linear combination of basis functions Taylor (58). Firstly, consider the case when  $\tilde{F}$  is univariate. There are many types of basis functions to parameterize a univariate function, such as polynomial basis, Fourier basis, and wavelet basis. Based on the observations from Theorem 1,  $\tilde{F}$  and  $F$  are expected to match only on a domain of  $u$  where the gray-box space-time solution exists and has large variation. Besides,  $\tilde{F}$  may match  $F$  better on a domain where the gray-box discretized solution  $\mathbf{u}$  are more densely sampled. Therefore, an ideal parameterization should admit local refinements so  $\tilde{F}$  can match  $F$  better at some domain; similarly, it should allow local dropouts when bases are redundant at some domain. This section presents a choice of the parameterization for  $\tilde{F}$  that allows such local refinements, while a procedure for basis refinement is given in the next section.

A parameterization that allows local refinements and local dropouts is the wavelet. Wavelet is the basis developed for multi-resolution analysis (MRA) Mallat (89). MRA is an increasing sequence of closed function spaces  $\{V_j\}_{j \in \mathbb{Z}}$ ,

$$\cdots \subset V_{-1} \subset V_0 \subset V_1 \subset \cdots,$$

which can approximate functions with increasing resolutions as  $j$  increases. For univariate MRA,  $V_j$ 's satisfy the following properties known as self-similarity:

$$\begin{aligned} f(u) \in V_j &\Leftrightarrow f(2u) \in V_{j+1}, \quad j \in \mathbb{Z} \\ f(u) \in V_j &\Leftrightarrow f(u - \frac{\eta}{2^j}) \in V_j, \quad j \in \mathbb{Z}, \eta \in \mathbb{Z} \end{aligned}$$

The wavelet bases for  $V_j$  are given by

$$\hat{\phi}_{j,\eta}(u) = 2^{j/2} \hat{\phi}(2^j u - \eta), \quad \eta \in \mathbb{Z} \quad (4.6)$$

where  $\hat{\phi}$  is called the mother wavelet satisfying  $\hat{\phi}(u) \rightarrow 0$  for  $u \rightarrow -\infty$  and  $\infty$ . An example mother wavelet, the Meyer wavelet, is shown in Figure 5.

Because the gray-box model is unchanged by adding a constant to  $F$ , the derivative of  $\tilde{F}$ , instead of  $\tilde{F}$  itself, should be approximated. Thereby, the bases for  $\tilde{F}$  shall be chosen as the integrals of the wavelets, i.e.

$$\phi_{j,\eta}(u) = \int_{-\infty}^u \hat{\phi}_{j,\eta}(u') du'. \quad (4.7)$$

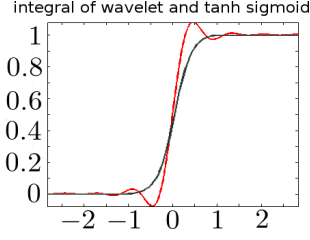


Figure 6: Red line: the integral (4.7) of the Meyer wavelet. Black line: the logistic sigmoid function.

$\phi_{j,\eta}$ 's are sigmoid functions which satisfy

$$\phi_{j,\eta}(u) = \begin{cases} 0, & u \rightarrow -\infty \\ 1, & u \rightarrow \infty \end{cases} \quad (4.8)$$

It's easy to show  $\phi_{j,\eta}$  also satisfies self-similarity, and can be represented by a mother sigmoid  $\phi$ ,

$$\phi_{j,\eta}(u) = \phi(2^j u - \eta), \quad j \in \mathbb{Z}, \eta \in \mathbb{Z} \quad (4.9)$$

There are many types of sigmoid functions. The article will use the logistic sigmoid function as the mother sigmoid,

$$\phi(u) = \frac{1}{1 + e^{-u}}. \quad (4.10)$$

If  $\tilde{F}$  is univariate, the logistic sigmoids  $\phi_{j,\eta}$ 's are used as the bases. If  $\tilde{F}$  is multivariate, the basis can be formed by the tensor product of univariate sigmoids,

$$\phi_{\mathbf{j},\boldsymbol{\eta}}(u_1, \dots, u_k) = \phi_{j_1,\eta_1}(u_1) \cdots \phi_{j_k,\eta_k}(u_k), \quad (4.11)$$

where  $\mathbf{j} = (j_1, \dots, j_k) \in \mathbb{Z}^k$ ,  $\boldsymbol{\eta} = (\eta_1, \dots, \eta_k) \in \mathbb{Z}^k$ . To sum up,

$$\tilde{F}(\cdot) = \sum_{\mathbf{j},\boldsymbol{\eta}} \alpha_{\mathbf{j},\boldsymbol{\eta}} \phi_{\mathbf{j},\boldsymbol{\eta}}(\cdot), \quad (4.12)$$

where  $\alpha$ 's are the coefficients of the bases. A systematic procedure for choosing a set of  $\{\mathbf{j}, \boldsymbol{\eta}\}$  is presented in Section 4.3.

For illustration, consider a numerical example where the gray-box model solves the 1-D Buckley-Leverett equation Buckley (42)

$$\frac{\partial u}{\partial t} + \frac{\partial}{\partial x} \left( \underbrace{\frac{u^2}{1 + 2(1-u)^2}}_F \right) = c, \quad (4.13)$$

with the initial condition  $u(0, x) = u_0(x)$  and the periodic boundary condition  $u(t, 0) = u(t, 1)$ . Let  $0 \leq u_0(x) \leq 1$  for all  $x \in [0, 1]$ . This is because the Buckley-Leverett equation models the two-phase porous media flow where  $u$  stands for the saturation of a phase, and the saturation is always positive and no larger than one.  $c \in \mathbb{R}$  is a constant-valued control.  $F$  is assumed unknown and is inferred by a twin model. The twin model solves

$$\frac{\partial \tilde{u}}{\partial t} + \frac{\partial}{\partial x} \tilde{F}(\tilde{u}) = c, \quad (4.14)$$

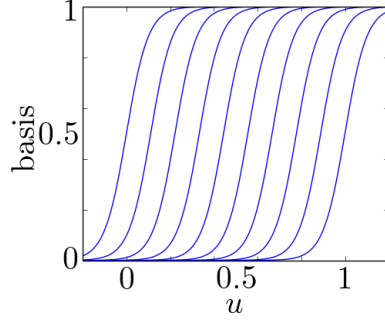


Figure 7: An ad hoc set of bases

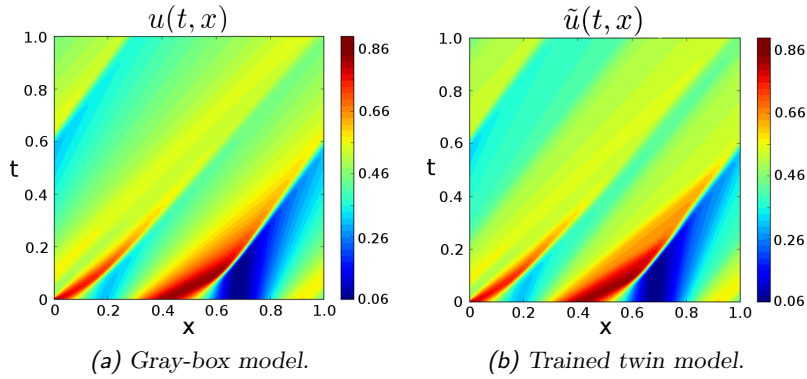


Figure 8: Space time solutions.

with the same  $c$  and the same initial and boundary conditions.  $\tilde{F}$  is parameterized by (4.12) where  $j$ 's and  $\eta$ 's are chosen ad hoc. Figure 7 gives an example of the bases used in this section. To ensure the well-posedness of (4.3), an ad hoc  $L_1$  regularization on  $\alpha$  is used in minimizing  $\mathcal{M}$ .

Figure 8a shows the discretized space-time solution of (4.13) for  $x \in [0, 1]$ ,  $t \in [0, 1]$  and  $c = 0$ . The solution is used to train a twin model according to (4.3). The discretized space-time solution of the trained twin model is shown in Figure 8b.

Once a twin model is trained, its adjoint can be used for gradient estimation. Consider an objective function

$$\xi(c) \equiv \int_{x=0}^1 \left( u(1, x; c) - \frac{1}{2} \right)^2 dx. \quad (4.15)$$

Its gradient  $\frac{d\xi}{dc}$  can be estimated by the trained twin model. Figure 9 shows the objective function, evaluated using the gray-box model and the trained twin model. It is observed that the gradients of  $\xi$  match closely at  $c = 0$ , i.e. the control where the twin model is trained.

In addition to the gradient estimation, the inferred  $\tilde{F}$  is examined. If different solutions are used in the training, it is expected that the trained twin model will also be different. Figure 10 shows the training results for three different initial conditions. Some

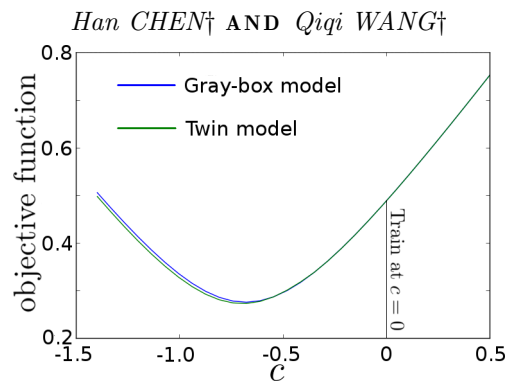


Figure 9: The objective function  $\xi$  evaluated by either the gray-box model or the trained twin model.

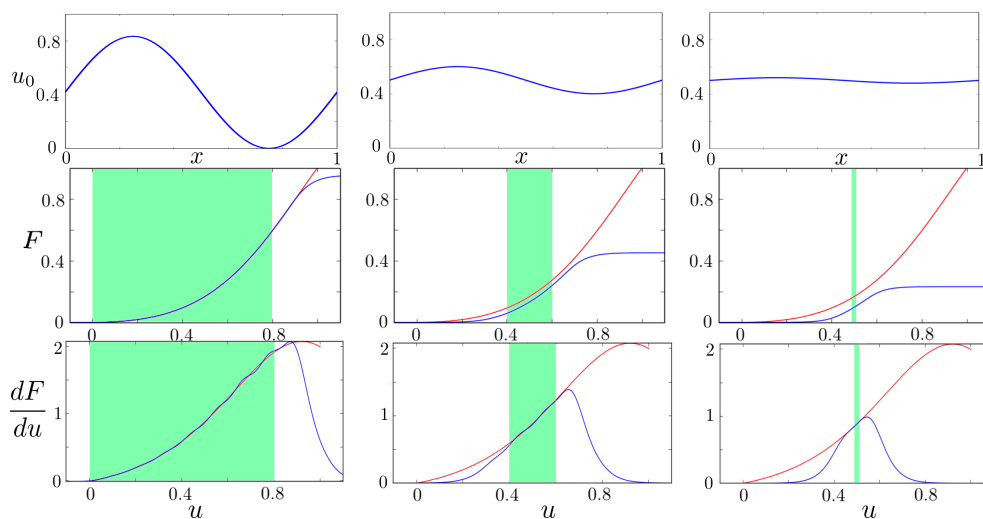


Figure 10: The first row shows the three different initial conditions used to generate the gray-box space-time solution. The second row compares the trained  $\tilde{F}$  (blue) and the Buckley-Leverett  $F$  (red). The third row compares the trained  $\frac{d\tilde{F}}{du}$  (blue) and the Buckley-Leverett  $\frac{dF}{du}$  (red). The green background highlights the domain of  $u$  where the gray-box space-time solution exists.

observations can be made: 1) As expected,  $\tilde{F}$  can differ from  $F$  by a constant without affecting  $\mathcal{M}$ ; 2)  $\frac{d\tilde{F}}{du}$  matches  $\frac{dF}{du}$  only in a domain of  $u$  where the solution exists (indicated by the green area); 3) Sometimes the bases seem redundant thus can be safely dropped out. The issue seems particularly important in the third column, where most bases are suppressed; 4) Sometime the bases seem too coarse thus may be refined in order to reduce the minimal  $\mathcal{M}$ . The issue seems particularly important in the first column, where  $\frac{d\tilde{F}}{du}$  exhibits a wavy deviation from  $\frac{dF}{du}$ . Addressing these issues systematically is crucial to the rigorous development of the twin model method.

### 4.3. Elements for Adaptive Basis Construction

This section develops several key elements that lead to the adaptive basis construction for twin models. The heuristics for the adaptive basis construction, discussed in Section 3.3, are applied to build up a basis dictionary consisted of only the significant candidates. The section is organized as follows: Firstly, a formulation is provided to efficiently assess the significance of each candidate basis; Secondly, the neighborhood of a sigmoid basis is defined; Thirdly, a metric is devised that determines when to add or remove a candidate basis. The three elements are then employed to build the twin model algorithm in Section 4.4.

Given a basis dictionary  $\phi_{\mathcal{A}} = \{\phi_i\}_{i \in \mathcal{A}}$ , define the “minimal mismatch”

$$\mathcal{M}^*(\mathcal{A}) = \min_{\alpha_{\mathcal{A}} \in \mathbb{R}^{|\mathcal{A}|}} \mathcal{M} \left( \sum_{i \in \mathcal{A}} \alpha_i \phi_i \right), \quad (4.16)$$

to be the minimal solution mismatch (4.2) if  $\tilde{F}$  were parameterized by  $\phi_{\mathcal{A}}$ .  $\mathcal{A}$  is a set containing  $\{j, \eta\}$ 's.  $\alpha_{\mathcal{A}} = \{\alpha_i\}_{i \in \mathcal{A}}$  is the coefficient for  $\phi_{\mathcal{A}}$ . Let  $\alpha_{\mathcal{A}}^* = \{\alpha_i^*\}_{i \in \mathcal{A}}$  be the optimal coefficients, and let  $\tilde{F}_{\mathcal{A}}^* = \sum_{i \in \mathcal{A}} \alpha_i^* \phi_i$ . Consider appending  $\phi_{\mathcal{A}}$  by an additional basis  $\phi_l$ , and let  $\phi_{\mathcal{A}'} = \{\phi_{\mathcal{A}}, \phi_l\}$ ,  $\mathcal{A}' = \{\mathcal{A}, l\}$ . The minimal mismatch for the appended basis dictionary  $\phi_{\mathcal{A}'}$  is

$$\mathcal{M}^*(\mathcal{A}') = \min_{\alpha_{\mathcal{A}'} \in \mathbb{R}^{|\mathcal{A}'|+1}} \mathcal{M} \left( \sum_{i \in \mathcal{A}'} \alpha_i \phi_i \right), \quad (4.17)$$

Clearly  $\mathcal{M}^*(\mathcal{A}') \leq \mathcal{M}^*(\mathcal{A})$ . Define the “mismatch improvement” to be

$$\Delta \mathcal{M}^*(\mathcal{A}, l) = \mathcal{M}^*(\mathcal{A}) - \mathcal{M}^*(\mathcal{A}') \quad (4.18)$$

Approximate (4.18) by Taylor expansion, we get

$$\Delta \mathcal{M}^*(\mathcal{A}, l) \approx - \left( \int_{u \in \mathbb{R}^k} \frac{d\mathcal{M}}{d\tilde{F}} \Big|_{\tilde{F}_{\mathcal{A}}^*} \phi_l du \right) \alpha_l, \quad (4.19)$$

where  $\frac{d\mathcal{M}}{d\tilde{F}}$  is the derivative of  $\mathcal{M}(\tilde{F})$  with respect to  $\tilde{F}$ , evaluated on  $\tilde{F} = \tilde{F}_{\mathcal{A}}^*$ . For a twin model consisted of a system of  $k$  equations,  $\tilde{F}$  is a function of  $u \in \mathbb{R}^k$ , thus  $\frac{d\mathcal{M}}{d\tilde{F}}$  is also a function of  $u \in \mathbb{R}^k$ . As discussed in the previous sections,  $\frac{d\mathcal{M}}{d\tilde{F}}$  is non-zero only in a domain where there is solution. Thus (4.19) can be integrated by quadrature only over a bounded domain. The absolute value of the coefficient for  $\alpha_l$ ,

$$s_l(\mathcal{A}) \equiv \left| \int_{u \in \mathbb{R}^k} \frac{d\mathcal{M}}{d\tilde{F}} \Big|_{\tilde{F}_{\mathcal{A}}^*} \phi_l du \right|, \quad (4.20)$$

estimates the significance of the basis  $\phi_l$  Miller (90). If there are multiple candidate bases, (4.20) can be used to rank their significance.

In the sequel, a compact representation of the sigmoid bases is introduced. The univariate basis function,  $\phi_{j, \eta}$  in (4.9), is represented by a tuple  $(j, \frac{\eta}{2^j})$ , where  $j$  can be viewed as the “resolution”, and  $\frac{\eta}{2^j}$  is the center of the basis. Similarly, the  $k$ -variate basis function,  $\phi_{j, \eta}$  in (4.11), is represented by a tuple  $(j, \frac{\eta}{2^j}) = (j_1, \dots, j_k, \{\frac{\eta_1}{2^{j_1}}, \dots, \frac{\eta_k}{2^{j_k}}\})$ . Thus,

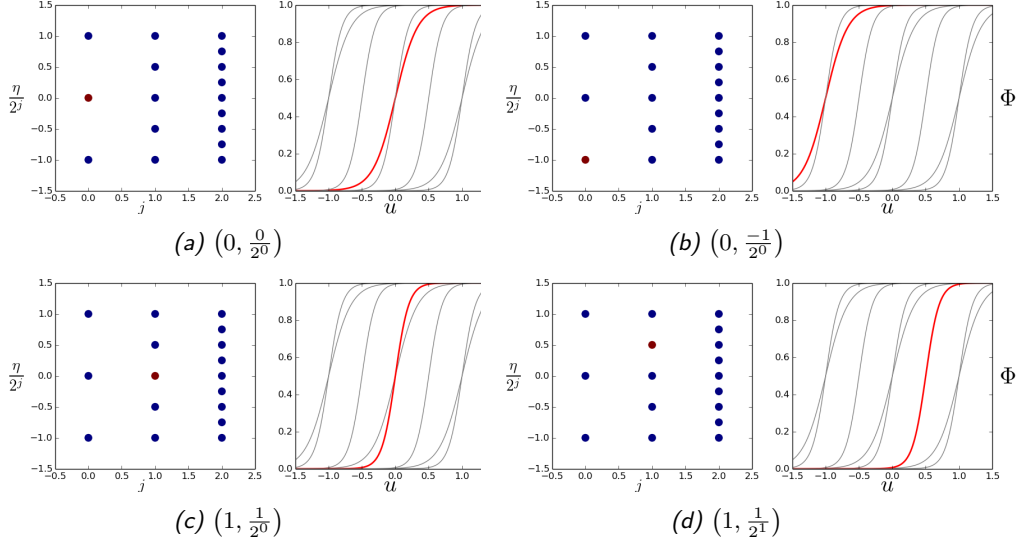


Figure 11: An illustration of the tuple representation and the corresponding univariate sigmoid.

a sigmoid can be represented by a point in a  $2k$ -dimensional space. The representation is illustrated in Figure 11a thru. 11d for the univariate case.

Using this representation, define the “neighborhood” of a univariate sigmoid  $(j, \frac{\eta}{2^j})$  to be

$$\mathcal{N} \left[ \left( j, \frac{\eta}{2^j} \right) \right] = \left\{ \left( j+1, \frac{\eta}{2^j} \right), \left( j, \frac{\eta \pm 1}{2^j} \right) \right\}. \quad (4.21)$$

The neighborhood contains 1) a basis  $(j+1, \frac{\eta}{2^j})$  with an increment of resolution; and 2) two basis  $(j, \frac{\eta \pm 1}{2^j})$  with the same resolution but a marginal shift of center. For illustration, the neighborhood of  $(0, \frac{0}{2^0})$  is shown in Figure 12a. Similarly, define the neighborhood of a multivariate sigmoid to be

$$\begin{aligned} \mathcal{N} \left[ \left( \mathbf{j}, \frac{\boldsymbol{\eta}}{2^{\mathbf{j}}} \right) \right] &= \mathcal{N} \left[ \left( \{j_1, \dots, j_k\}, \left\{ \frac{\eta_1}{2^{j_1}}, \dots, \frac{\eta_k}{2^{j_k}} \right\} \right) \right] \\ &= \left\{ \left( \{j_1+1, \dots, j_k\}, \left\{ \frac{\eta_1}{2^{j_1+1}}, \dots, \frac{\eta_k}{2^{j_k}} \right\} \right), \dots, \left( \{j_1, \dots, j_k+1\}, \left\{ \frac{\eta_1}{2^{j_1}}, \dots, \frac{\eta_k}{2^{j_k+1}} \right\} \right), \right. \\ &\quad \left. \left( \{j_1, \dots, j_k\}, \left\{ \frac{\eta_1 \pm 1}{2^{j_1}}, \dots, \frac{\eta_k}{2^{j_k}} \right\} \right), \dots, \left( \{j_1, \dots, j_k\}, \left\{ \frac{\eta_1}{2^{j_1}}, \dots, \frac{\eta_k \pm 1}{2^{j_k}} \right\} \right) \right\}, \end{aligned} \quad (4.22)$$

which consists of  $k$  bases with incremental resolution, and  $2k$  bases with center shifts. It is easy to see that a basis  $(\mathbf{j}_0, \frac{\boldsymbol{\eta}_0}{2^{\mathbf{j}_0}})$  can be connected to any basis  $(\mathbf{j}, \frac{\boldsymbol{\eta}}{2^{\mathbf{j}}})$  with  $\mathbf{j} \geq \mathbf{j}_0$  through a chain of neighborhoods. In addition, define the neighborhood of multiple sigmoid functions to be the union of each individual’s neighborhood, as illustrated by Figure 12b.

$$\mathcal{N} \left[ \left( \mathbf{j}_1, \frac{\boldsymbol{\eta}_1}{2^{\mathbf{j}_1}} \right), \dots, \left( \mathbf{j}_n, \frac{\boldsymbol{\eta}_n}{2^{\mathbf{j}_n}} \right) \right] = \mathcal{N} \left[ \left( \mathbf{j}_1, \frac{\boldsymbol{\eta}_1}{2^{\mathbf{j}_1}} \right) \right] \cup \dots \cup \mathcal{N} \left[ \left( \mathbf{j}_n, \frac{\boldsymbol{\eta}_n}{2^{\mathbf{j}_n}} \right) \right]. \quad (4.23)$$

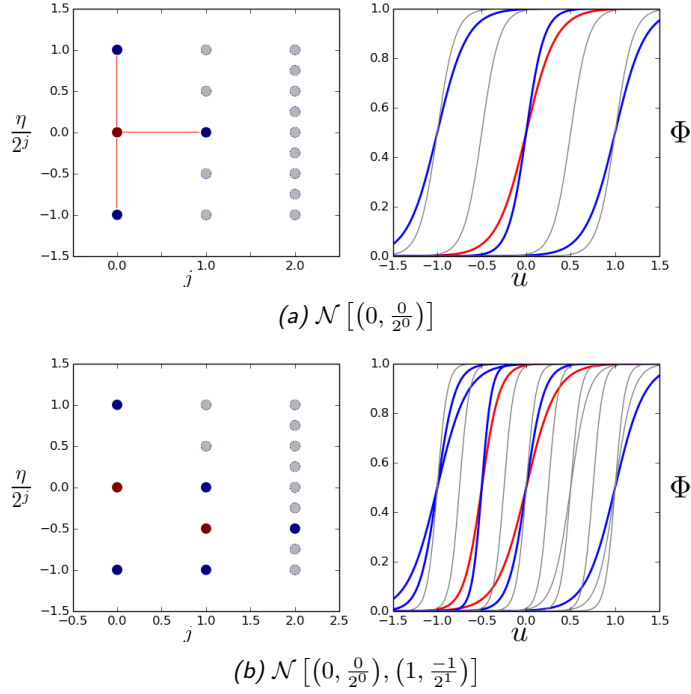


Figure 12: Neighborhood for univariate bases. (a) shows the neighborhood (blue) of a single basis (red). (b) shows the neighborhood (blue) of several bases (red). The left column represents the basis on the  $(j, \frac{\eta}{2^j})$  plane, and the right column shows the actual basis  $\phi_{j,\eta}$ .

Although the mismatch improvement,  $\Delta \mathcal{M}^*(\mathcal{A}, l)$ , is always non-negative, it is inadvisable to cram the basis dictionary with too many bases, otherwise a twin model can be overfitted. Therefore, a criterion is required to determine if a candidate basis shall be added to or removed from the basis dictionary. This can be achieved by cross validation, in particular,  $k$ -fold cross validation Geisser (93). Given a basis dictionary, the  $k$ -fold cross validation proceeds in the following three steps: Firstly, the gray-box solution  $\mathbf{u}$  is shuffled randomly into  $k$  disjoint sets  $\{\mathbf{u}_1, \mathbf{u}_2, \dots, \mathbf{u}_k\}$ . An illustration for  $k = 2$  is shown in Figure 13.

Secondly,  $k$  twin models who share the same basis dictionary are trained so their space-time solutions match all but one sets, shown in (4.24).  $T_i$  indicates the  $i$ th twin model.

$$\begin{aligned}
 T_1 &= \text{TrainTwinModel}(\mathbf{u}_2, \mathbf{u}_3, \dots, \mathbf{u}_k) \\
 T_2 &= \text{TrainTwinModel}(\mathbf{u}_1, \mathbf{u}_3, \dots, \mathbf{u}_k) \\
 &\dots \\
 T_k &= \text{TrainTwinModel}(\mathbf{u}_1, \mathbf{u}_2, \dots, \mathbf{u}_{k-1})
 \end{aligned} \tag{4.24}$$

Thirdly, each trained twin model is validated on the remaining set. In particular, the

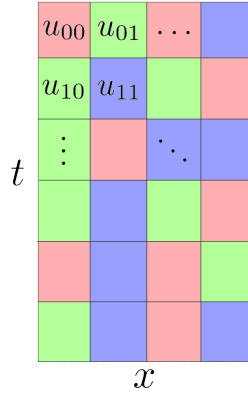


Figure 13: The discretized gray-box solution is shuffled into 3 sets, each indicated by a color.

solution mismatch for the validation set is computed, as shown in (4.25).

$$\begin{aligned}
 \mathcal{M}_1 &= \text{MismatchValidation}(T_1, \mathbf{u}_1) \\
 \mathcal{M}_2 &= \text{MismatchValidation}(T_2, \mathbf{u}_2) \\
 &\dots \\
 \mathcal{M}_k &= \text{MismatchValidation}(T_k, \mathbf{u}_k)
 \end{aligned} \tag{4.25}$$

The mean value of validation errors,

$$\overline{\mathcal{M}} = \frac{1}{k} (\mathcal{M}_1 + \mathcal{M}_2 + \dots + \mathcal{M}_k) \tag{4.26}$$

measures the performance of the basis dictionary. A basis shall be added to or removed from the dictionary only if such action reduces  $\overline{\mathcal{M}}$ . In practice, cross validation proliferates the computational cost. Therefore, a small  $k$  is preferable if cost is a concern. All the numerical examples in this article use  $k = 2$ .



## 4.4. Algorithm

Based upon the developments in the previous sections, a twin model algorithm with adaptive basis construction is devised.

**Input:** Initial basis dictionary  $\phi_{\mathcal{A}}$ , coefficients  $\alpha_{\mathcal{A}} = \mathbf{0}$ , Validation error  $\overline{\mathcal{M}}_0 = \infty$ , Gray-box solution  $\mathbf{u}$ .

- 1: Minimize solution mismatch  $\alpha_{\mathcal{A}} \leftarrow \operatorname{argmin}_{\alpha} \mathcal{M}(\sum_{i \in \mathcal{A}} \alpha_i \phi_i)$
- 2: **loop**
- 3:     Find  $\phi_l \in \mathcal{N}(\phi_{\mathcal{A}}) \setminus \phi_{\mathcal{A}}$  with the maximal  $s_l(\mathcal{A})$   
 $\mathcal{A} \leftarrow \mathcal{A} \cup \{l\}$ ,  $\phi_{\mathcal{A}} \leftarrow \phi_{\mathcal{A}} \cup \{\phi_l\}$ ,  $\alpha_l = 0$ ,  $\alpha_{\mathcal{A}} \leftarrow \{\alpha_{\mathcal{A}}, \alpha_l\}$
- 4:     Compute  $\overline{\mathcal{M}}$  by  $k$ -fold cross validation.
- 5:     **if**  $\overline{\mathcal{M}} < \overline{\mathcal{M}}_0$  **then**
- 6:          $\overline{\mathcal{M}}_0 \leftarrow \overline{\mathcal{M}}$   
 $\alpha_{\mathcal{A}} \leftarrow \operatorname{argmin}_{\alpha} \mathcal{M}(\sum_{i \in \mathcal{A}} \alpha_i \phi_i)$
- 7:     **else**
- 8:          $\mathcal{A} \leftarrow \mathcal{A} \setminus \{l\}$ ,  $\phi_{\mathcal{A}} \leftarrow \phi_{\mathcal{A}} \setminus \{\phi_l\}$ ,  $\alpha_{\mathcal{A}} \leftarrow \alpha_{\mathcal{A}} \setminus \{\alpha_l\}$  **break**
- 9:     **end if**
- 10:    Find  $\phi_{l'} \in \phi_{\mathcal{A}}$  with the least  $s_{l'}(\mathcal{A})$
- 11:    **if**  $l' \neq l$  **then**
- 12:        $\mathcal{A} \leftarrow \mathcal{A} \setminus \{l'\}$ ,  $\phi_{\mathcal{A}} \leftarrow \phi_{\mathcal{A}} \setminus \{\phi_{l'}\}$ ,  $\alpha_{\mathcal{A}} \leftarrow \alpha_{\mathcal{A}} \setminus \{\alpha_{l'}\}$
- 13:       Compute  $\overline{\mathcal{M}}$  by  $k$ -fold cross validation.
- 14:       **if**  $\overline{\mathcal{M}} < \overline{\mathcal{M}}_0$  **then**
- 15:            $\overline{\mathcal{M}}_0 \leftarrow \overline{\mathcal{M}}$   
 $\alpha_{\mathcal{A}} \leftarrow \operatorname{argmin}_{\alpha} \mathcal{M}(\sum_{i \in \mathcal{A}} \alpha_i \phi_i)$
- 16:       **else**
- 17:            $\mathcal{A} \leftarrow \mathcal{A} \cup \{l'\}$ ,  $\phi_{\mathcal{A}} \leftarrow \phi_{\mathcal{A}} \cup \{\phi_{l'}\}$ ,  $\alpha_{\mathcal{A}} \leftarrow \alpha_{\mathcal{A}} \cup \{\alpha_{l'}\}$
- 18:       **end if**
- 19:    **end if**
- 20: **end loop**

**Output:**  $\mathcal{A}$ ,  $\phi_{\mathcal{A}}$ ,  $\alpha_{\mathcal{A}}$ .

**Algorithm 1:** Training twin model with adaptive basis construction.

Algorithm 1 adopts the heuristics of the forward-backward iteration discussed in Section 3.3. The algorithm starts from training a twin model using a simple basis dictionary. Usually the starting dictionary contains one basis for each dimension with very low resolution. Details of the choice are given in Section 5 along with numerical examples. The main part of the algorithm iterates over a forward step (line 3-9) and a backward step (line 10-19). The forward step firstly finds the most promising candidate in the neighborhood of the current dictionary for addition, according to (4.20). If the addition indeed reduces the cross validation error, the candidate is appended to the dictionary; otherwise it is rejected. If the basis is appended, the coefficients are updated by minimizing the solution mismatch, which can be implemented by the Broyden-Fletcher-Goldfarb-Shannon (BFGS) algorithm Dennis (77). The backward step finds the most promising candidate in the current dictionary for deletion. If the deletion reduces the cross validation error, the candidate is removed from the dictionary. If the basis is deleted, the coefficients are updated by BFGS again. The iteration exits when the most promising addition no longer reduces the validation error. In the end, the algorithm provides the basis dictionary and its coefficients as the output.

The algorithm requires to train multiple twin models at each iteration. For  $k = 2$ , 6 twin models are trained if both the forward and the backward step are acceptable. In practice, the trained coefficients at the last iteration usually provide good initial guess for the next iteration. Nonetheless, the algorithm can be costly if the dictionary turns out to have a high cardinality which results in a large number of iterations before the dictionary construction completes. Therefore, a numerical shortcut is provided in Section 4.5 that significantly reduces the cost.

#### 4.5. Minimizing the Truncation Error

In the previous sections, a twin model is trained to minimize the solution mismatch. The training can be expensive. Because the minimization of the solution mismatch, coupled with the adaptive basis construction, can require a large number of solution mismatch evaluations, and each evaluation involves one twin model simulation. To reduce the computational cost, a “pre-training” step is proposed where an “integrated truncation error” is minimized. A pre-trained twin model is then “fine tuned” to minimize the solution mismatch. The applicability of the pre-training is studied; in particular, I study under what condition can the solution mismatch be bounded by the integrated truncation error. Finally, a stochastic gradient descent approach is adopted that efficiently minimizes the integrated truncation error.

Define

$$\tau = \frac{\partial u}{\partial t} + \nabla \cdot (D\tilde{F}(u)) - q(u, c), \quad (4.27)$$

which is the residual if the gray-box PDE’s solution is plugged in the twin-model PDE (4.1). Let its discretization be  $\boldsymbol{\tau}$ . For simplicity, assume the gray-box simulator and its twin model use the same space-time discretization.  $\boldsymbol{\tau}$  can be obtained by plugging the discretized gray-box solution in the twin model simulator. Define the integrated truncation error to be

$$\mathcal{T}(\tilde{F}) = \sum_{i=1}^M \sum_{j=1}^N w_{ij} \boldsymbol{\tau}_{ij}^2, \quad (4.28)$$

where  $w_{ij}$  are the same quadrature weights as in (4.2).  $i, j$  are the indices for time and space discretization as in the previous sections. I propose to pre-train a twin model using Algorithm 1 with  $\mathcal{M}$  replaced by  $\mathcal{T}$ . In other words, in the pre-training step, the coefficients are determined by

$$\alpha_{\mathcal{A}} \leftarrow \underset{\alpha}{\operatorname{argmin}} \mathcal{T} \left( \sum_{i \in \mathcal{A}} \alpha_i \phi_i \right). \quad (4.29)$$

Besides, the estimator for the significance of a candidate basis,  $s_l(\mathcal{A})$ , is replaced by

$$s_l^t(\mathcal{A}) \equiv \left| \int_{u \in \mathbb{R}^k} \frac{d\mathcal{T}}{d\tilde{F}} \Big|_{\tilde{F}_{\mathcal{A}}^*} \phi_l \, du \right|. \quad (4.30)$$

Finally, the validation error,  $\overline{\mathcal{M}}$ , is replaced by

$$\overline{\mathcal{T}} = \frac{1}{k} (\mathcal{T}_1 + \mathcal{T}_2 + \cdots + \mathcal{T}_k), \quad (4.31)$$

where

$$\mathcal{T}_i = \text{IntegratedTruncationError}(T_i, \mathbf{u}_i). \quad (4.32)$$

for  $i = 1, \dots, k$ . Using the pre-trained basis dictionary  $\phi_{\mathcal{A}}^t$ , the twin model is then fine tuned by minimizing the solution mismatch, where  $\alpha_{\mathcal{A}}^t$  is used as the initial guess and is adjusted according to (4.3). For a simulation with implicit schemes, the residual and the integrated truncation error are cheaper to evaluate than the solution mismatch, thereby the benefit of the pre-train.

However,  $\mathcal{M}$  may not be bounded by  $\mathcal{T}$ . A sufficient condition under which the bound exists is provided by Theorem 2.

**THEOREM 2.** *Consider a twin model simulator whose one-step time marching is*

$$\mathcal{G}_i : \mathbb{R}^N \mapsto \mathbb{R}^N, \tilde{\mathbf{u}}_i \rightarrow \tilde{\mathbf{u}}_{i+1} = \mathcal{G}_i \tilde{\mathbf{u}}_i, \quad i = 1, \dots, M-1. \quad (4.33)$$

*Assume the quadrature weights are time-independent, i.e.  $w_{ij} = w_j$  for all  $i, j$ . If  $\mathcal{G}_i$  satisfies*

$$\|\mathcal{G}_i a - \mathcal{G}_i b\|_W^2 \leq \beta \|a - b\|_W^2, \quad (4.34)$$

*with  $\beta < 1$ , for any  $a, b \in \mathbb{R}^N$  and for all  $i$ , then*

$$\mathcal{M} \leq \frac{1}{1-\beta} \mathcal{T}, \quad (4.35)$$

*where*

$$\|v\|_W^2 \equiv v^T \begin{pmatrix} w_1 & & \\ & \ddots & \\ & & w_N \end{pmatrix} v \quad (4.36)$$

*for any  $v \in \mathbb{R}^N$ .*

The proof is given in Appendix 7.2. If the twin model is a contractive dynamical system Lohmiller (98), as given by (4.34), then the solution mismatch can be bounded by the integrated truncation error. In contrast, the bound may not exist for non-contractive dynamical systems, for example for systems that exhibit bifurcation. It is a future work to further investigate the applicability of the pre-training theoretically, in particular, to investigate the necessary and sufficient condition for the bound. This article will explore the usefulness of the pre-training by several numerical test cases.

Because the residual  $\boldsymbol{\tau}$  can be evaluated explicitly given the gray-box solution, the evaluation can be decoupled for different space-time grid points  $\{i, j\}$ . By viewing the truncation error at each  $\{i, j\}$  as a stochastic sample, (4.29) can be solved by stochastic gradient descent, Algorithm 2.

$\lambda > 0$  is a tunable step size.  $\lambda$  can be tuned manually to increase convergence speed while avoiding divergence Spall (05). In practice, it is beneficial to compute the gradient against more than one grid points (called a ‘‘mini-batch’’) at each iteration. This is because the code can take advantage of vectorization libraries rather than computing the residual at each grid point separately.

**Input:**  $\alpha = \alpha_0$   
 1: **for**  $(i, j) = (1, 1)$  **to**  $(M, N)$  **do**  
 2:     **if** not converged **then**  
 3:          $\alpha \leftarrow \alpha - \lambda w_{ij} \frac{\partial}{\partial \alpha} \tau_{ij}$   
 4:     **else**  
 5:         **break**  
 6:     **end if**  
 7: **end for**

**Output:**  $\alpha$

**Algorithm 2:** Minimizing the integrated truncation error by stochastic gradient descent.

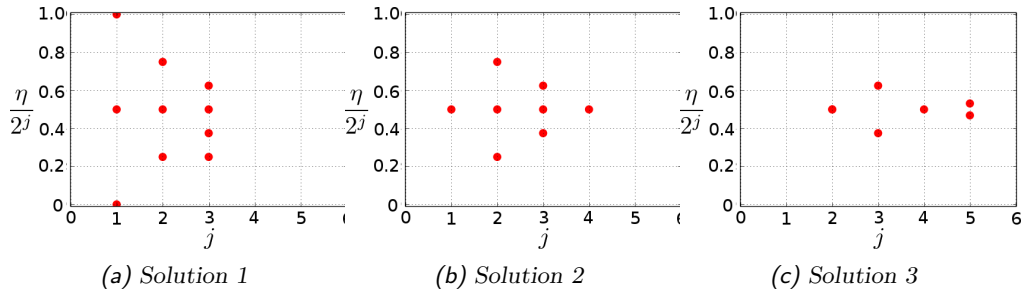


Figure 14: The basis dictionary for the three solutions in Figure 10.

## 5. Numerical Results

This section demonstrates the twin model on the estimation of the gradients for several numerical examples.

### 5.1. Buckley-Leverett Equation

Section 4.2 has applied a sigmoid parameterization to the gray-box model governed by the Buckley-Leverett equation (4.13). In this section, the same problem is studied but using the adaptive basis construction developed in Section 4.4 and 4.5. The initial dictionary,  $\phi_A$ , is selected to contain a single basis  $(0, \frac{0}{2^0})$ . Clearly the choice is not unique. As long as the initial basis has a low resolution and is centered around  $[u_{\min}, u_{\max}]$ , Algorithm 1 shall build the dictionary adaptively.

Figure 14 shows the selected bases for the three solutions in Figure 10, respectively, by using the pre-train step. As  $[u_{\min}, u_{\max}]$  shrinks, the dictionary's cardinality reduces and the resolution increases.

Consider a time-space-dependent control  $c = c(t, x)$  in (4.13) and (4.14). The gradient of  $\xi$ , (4.15), is estimated using the trained twin model. The estimated gradients are compared with the true adjoint gradients of the gray-box model, and the errors are shown in Figure 15.

The adaptive basis construction improves the accuracy of the gradient estimation. Table 1 shows the integrated gradient error <sup>†</sup> by using either the ad hoc bases in Figure 7

<sup>†</sup> The gradient error is integrated using the same quadrature rule as in (4.2).

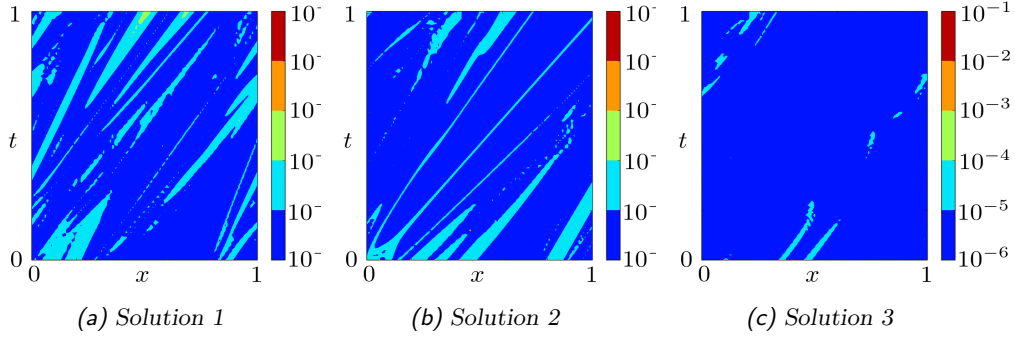


Figure 15: The errors of estimated gradients for the three solutions.

or by using the bases constructed adaptively.

	Solution 1	Solution 2	Solution 3
Ad hoc basis	$2.5 \times 10^{-3}$	$6.6 \times 10^{-4}$	$7.3 \times 10^{-5}$
Adaptive basis	$4.2 \times 10^{-6}$	$1.5 \times 10^{-6}$	$8.9 \times 10^{-7}$

Table 1: The integrated errors of the estimated gradients for the three solutions.

## 5.2. Navier-Stokes Flow

Consider a compressible internal flow in a 2-D return bend channel driven by the pressure difference between the inlet and the outlet. The return bend is bounded by no-slip walls. The inlet static pressure and the outlet pressure are fixed. The geometry of the return bend is given in Figure 16. The inner and outer boundaries of the bending section are each generated by 6 control points using quadratic B-spline.

The flow is governed by Navier-Stokes equations. Let  $\rho$ ,  $u$ ,  $v$ ,  $E$ , and  $p$  denote the density, Cartesian velocity components, total energy, and pressure. The steady-state Navier-Stokes equation is

$$\frac{\partial}{\partial x} \begin{pmatrix} \rho u \\ \rho u^2 + p - \sigma_{xx} \\ \rho uv - \sigma_{xy} \\ u(E\rho + p) - \sigma_{xx}u - \sigma_{xy}v \end{pmatrix} + \frac{\partial}{\partial y} \begin{pmatrix} \rho v \\ \rho v^2 + p - \sigma_{yy} \\ \rho uv - \sigma_{xy} \\ v(E\rho + p) - \sigma_{xy}u - \sigma_{yy}v \end{pmatrix} = \mathbf{0}, \quad (5.1)$$

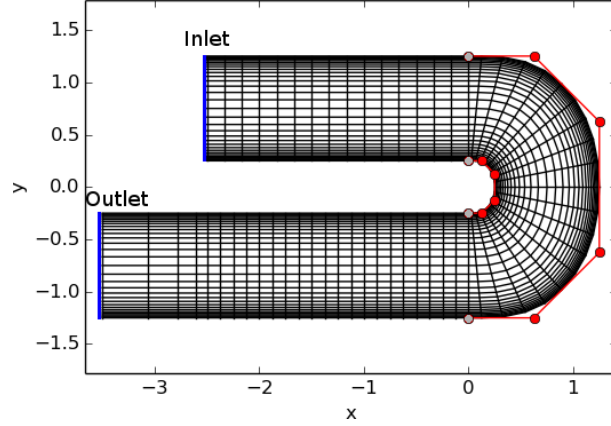


Figure 16: The return bend geometry and the mesh for the simulation.

where

$$\begin{aligned}\sigma_{xx} &= \mu \left( 2 \frac{\partial u}{\partial x} - \frac{2}{3} \left( \frac{\partial u}{\partial x} + \frac{\partial v}{\partial y} \right) \right) \\ \sigma_{yy} &= \mu \left( 2 \frac{\partial v}{\partial y} - \frac{2}{3} \left( \frac{\partial u}{\partial x} + \frac{\partial v}{\partial y} \right) \right) . \\ \sigma_{xy} &= \mu \left( \frac{\partial u}{\partial y} + \frac{\partial v}{\partial x} \right)\end{aligned}\quad (5.2)$$

The Navier-Stokes equation requires an additional equation, the state equation, for closure. The state equation has the form

$$p = p(U, \rho), \quad (5.3)$$

where  $U$  denotes the internal energy per unit volume,

$$U = \rho \left( E - \frac{1}{2}(u^2 + v^2) \right). \quad (5.4)$$

Many models have been developed for the state equation, such as the ideal gas equation, the van der Waals equation, and the Redlich-Kwong equation Murdock (93). In the sequel, the true state equation in the gray-box simulator is assumed unknown and will be inferred from the gray-box solution. Let  $\rho_\infty$  be the steady state density,  $\mathbf{u}_\infty = (u_\infty, v_\infty)$  be the steady state Cartesian velocity, and  $E_\infty$  be the steady state energy density. The steady state mass flux is

$$\xi = - \int_{\text{outlet}} \rho_\infty u_\infty |_{\text{outlet}} dy = \int_{\text{inlet}} \rho_\infty u_\infty |_{\text{inlet}} dy \quad (5.5)$$

The goal is to estimate the gradient of  $\xi$  to the red control points' coordinates.

Two state equations are tested: the ideal gas equation and the Redlich-Kwong equation, given by

$$\begin{aligned}p_{ig} &= (\gamma - 1)U \\ p_{rk} &= \frac{(\gamma - 1)U}{1 - b_{rk}\rho} - \frac{a_{rk}\rho^{5/2}}{((\gamma - 1)U)^{1/2}(1 + b_{rk}\rho)}\end{aligned}\quad (5.6)$$

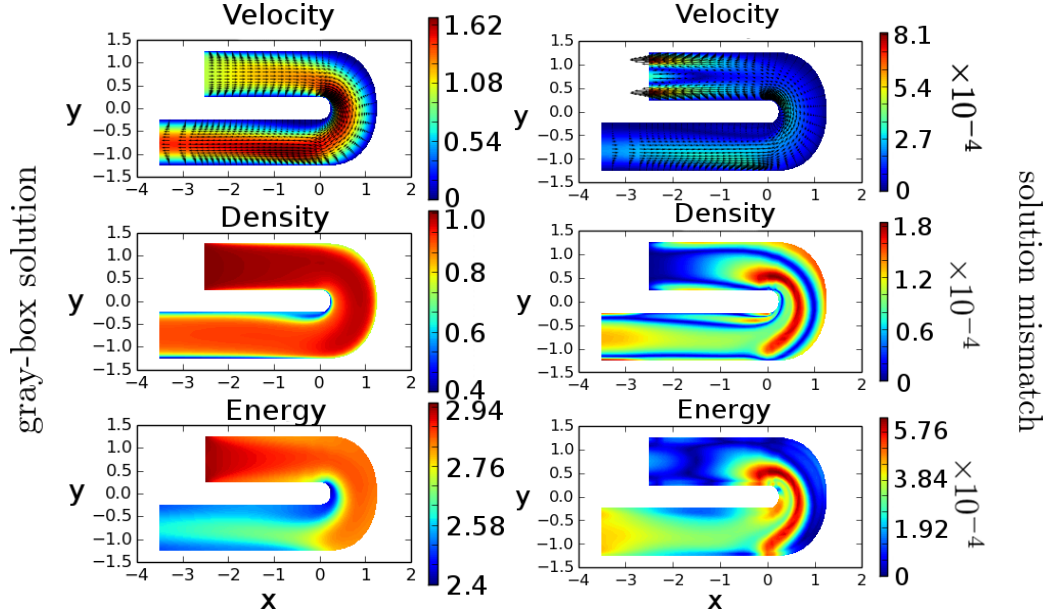


Figure 17: Left column: an example gray-box solution for a given geometry. Right column: the solution mismatch after training a twin model.

where  $a_{rk} = 10^7$  and  $b_{rk} = 0.1$ .

The solution mismatch, (4.2), is given by

$$\begin{aligned} \mathcal{M} = & w_\rho \int_{\Omega} |\tilde{\rho}_\infty - \rho_\infty|^2 d\mathbf{x} + w_u \int_{\Omega} |\tilde{u}_\infty - u_\infty|^2 d\mathbf{x} \\ & + w_v \int_{\Omega} |\tilde{v}_\infty - v_\infty|^2 d\mathbf{x} + w_E \int_{\Omega} |\tilde{E}_\infty - E_\infty|^2 d\mathbf{x}, \end{aligned}$$

where  $w_\rho$ ,  $w_u$ ,  $w_v$ , and  $w_E$  are non-dimensionalization constants. Figure 17 shows the gray-box solution and the solution mismatch after training the twin model †. Figure 18 compares the true state equation and the corresponding trained state equation, where the convex hull of  $(U_\infty, \rho_\infty)$ , the internal energy and the density of the gray-box solution, is shown by the dashed red line. Because the state equation is expected to be inferrable only inside the domain of the gray-box solution, large deviation is expected outside the convex hull.

The trained twin model enables the adjoint gradient estimation. Figure 19 shows the estimated gradient of  $\xi$  with respect to the control points coordinates. It also compares the estimated gradient with the true gradient. The two gradients are indistinguishable, and the error is given in Table 2.

† Both the solution and the mismatch are normalized.

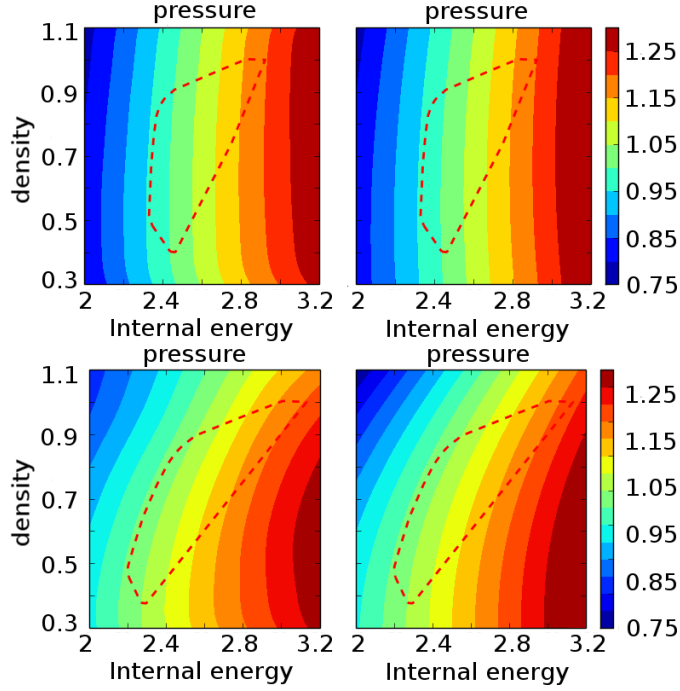


Figure 18: The gray-box state equation (right column) and the trained state equation (left column). The gray-box model uses either the ideal gas equation (first row) or the Redlich-Kwong equation (second row). The convex hull of the gray-box solution is shown by the dashed red line.

Gas	Interior control points				Exterior control points			
Ideal	0.13	0.04	0.05	0.32	0.16	0.15	0.07	0.02
Redlich-Kwong	0.32	0.03	0.07	0.50	0.40	0.12	0.06	0.05

Table 2: The error of the gradient estimation, in percentage.

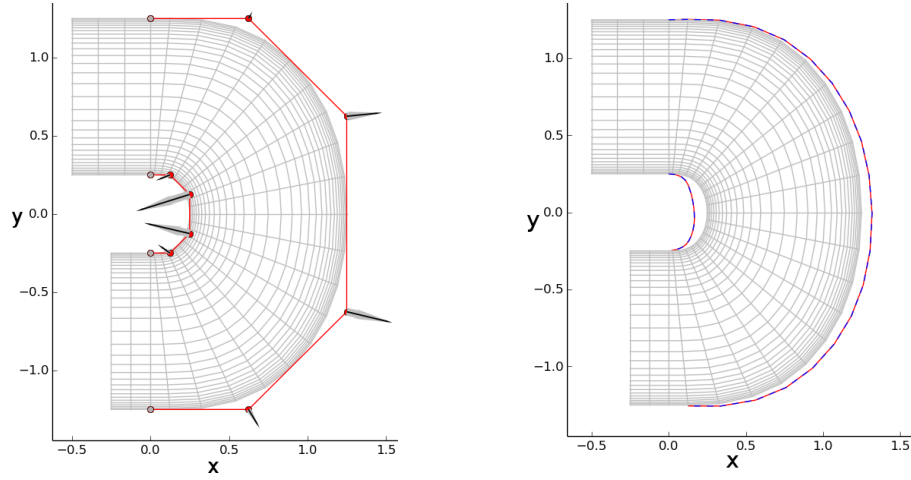
### 5.3. Polymer Injection in Petroleum Reservoir

Water flooding is a technique to enhance the secondary recovery in petroleum reservoirs, as illustrated in Figure 20. Injecting pure water can be cost-inefficient due to low water viscosity and high water cut. Therefore, water-solvent polymer can be utilized to increase the water-phase viscosity and to reduce the residual oil.

Consider a reservoir governed by the two-phase porous media flow equations

$$\begin{aligned}
 \frac{\partial}{\partial t} (\rho_\alpha \phi S_\alpha) + \nabla \cdot (\rho_\alpha \vec{v}_\alpha) &= 0, \quad \alpha \in \{w, o\} \\
 \frac{\partial}{\partial t} (\rho_w \phi S_w c) + \nabla \cdot (c \rho \vec{v}_{wp}) &= 0
 \end{aligned} \tag{5.7}$$





(a) The gradient of  $\xi$  to the control points for the Redlich-Kwong gas. The wide gray arrow is the gradient evaluated by the gray-box model, while the thin black arrow is the gradient evaluated by the twin model using finite difference.

(b) The boundary perturbed according to the gradient. The blue dashed line is computed by finite difference of the gray-box model, while the red dashed line is computed by the twin model's gradient.

Figure 19: A comparison of the estimated gradient and the true gradient.

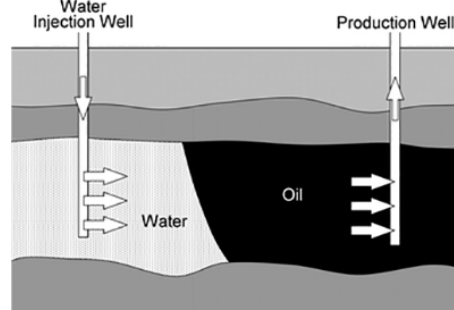


Figure 20: Water flooding in petroleum reservoir engineering (courtesy from PetroWiki).

for  $x \in \Omega$  and  $t \in [0, T]$ , where the phase velocities are given by the Darcy's law

$$\begin{aligned} \vec{v}_\alpha &= -M_\alpha k_{r\alpha} \mathbf{K} \cdot (\nabla p - \rho_w g \nabla z), \quad \alpha \in \{w, o\} \\ \vec{v}_{wp} &= -M_{wp} k_{rw} \mathbf{K} \cdot (\nabla p - \rho_w g \nabla z) \end{aligned} \quad (5.8)$$

$w, o$  indicate the water and oil phases.  $\rho$  is the phase density.  $\phi$  is the porosity.  $S$  is the phase saturation where  $S_w + S_o = 1$ .  $c$  is the polymer concentration in the water phase.  $v_w, v_o, v_{wp}$  are the componentwise velocities of water, oil, and polymer.  $\mathbf{K}$  is the permeability tensor.  $k_r$  is the relative permeability.  $p$  is the pressure.  $z$  is the depth.  $g$  is the gravity constant. The mobility factors,  $M_o, M_w, M_{wp}$ , model the modification of the componentwise mobility due to the presence of polymer. In the sequel, the models for the mobility factors are unknown. The only knowledge about the mobility factors is that

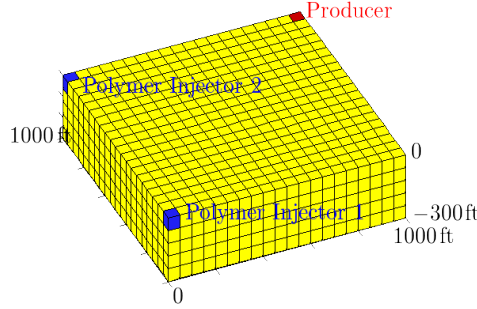


Figure 21: The geometry of the petroleum reservoir.

they depend on  $S_w$ ,  $p$ , and  $c$ .

*PSim*, the simulator aforementioned in Section 1, is used as the gray-box simulator, which uses the IMPES time marching, i.e. implicit in pressure and explicit in saturation, as well as the upwind scheme. Its solution,  $S_w$ ,  $c$ , and  $p$  can be used to train the twin model. The twin model uses fully implicit time marching and the upwind scheme. The solution mismatch is defined by

$$\mathcal{M} = w_{S_w} \int_0^T \int_{\Omega} |S_w - \tilde{S}_w|^2 d\mathbf{x} dt + w_c \int_0^T \int_{\Omega} |c - \tilde{c}|^2 d\mathbf{x} dt + w_p \int_0^T \int_{\Omega} |p - \tilde{p}|^2 d\mathbf{x} dt, \quad (5.9)$$

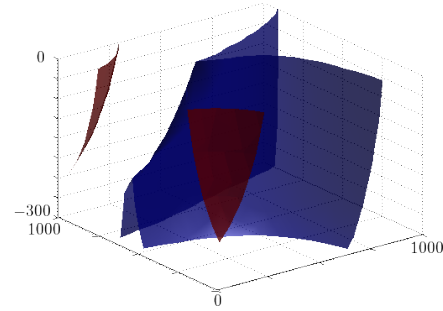
where  $w_{S_w}$ ,  $w_c$ , and  $w_p$  are non-dimensionalization constants.

Consider a reservoir setup shown in Figure 21, which is a 3D block with two injectors and one producer. The permeability is 100 milli Darcy, and the porosity is 0.3. A constant injection rate of  $10^6 \text{ft}^3/\text{day}$  is used at both the injectors. The reservoir is simulated for  $t \in [0, 50] \text{day}$ . The solution of  $S_w$  is illustrated in Figure 22 for the untrained twin model, the gray-box model, and the trained twin model, respectively. After the training, the twin-model solution matches the gray-box solution closely.

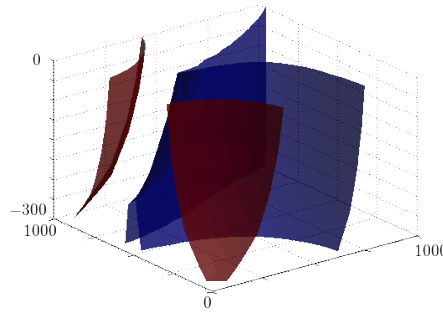
Let the objective function be the residual oil at  $T = 50 \text{day}$ ,

$$\xi = \int_{\Omega} \rho_o(T) \phi S_o(T) d\mathbf{x}. \quad (5.10)$$

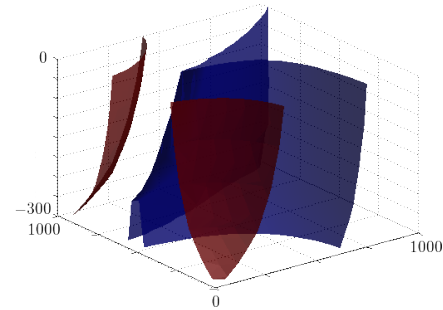
The gradient of  $\xi$  with respect to the time-dependent injection rate is computed. The gradient estimated by the twin model is shown in Figure 23, where the red and blue lines indicate the gradient for the two injectors. In comparison, the star markers show the true gradient at day 2, 16, 30, and 44, evaluated by finite difference. Clearly, a rate increase at the injector 1 leads to more residual oil reduction than the injector 2. This is because the injector 2 is closer to the producer, where a larger rate accelerates the water breakthrough that impedes further oil production. It is observed that the estimated gradient closely matches the true gradient, although the error slightly increases for smaller  $t$ , possibly because of the different numerical schemes used in the twin and gray-box models. The error is given in Table 3.



(a) Untrained twin model.



(b) PSim.



(c) Trained twin model.

Figure 22: The isosurfaces of  $S_w = 0.25$  and  $S_w = 0.7$  at  $t = 30$  days.

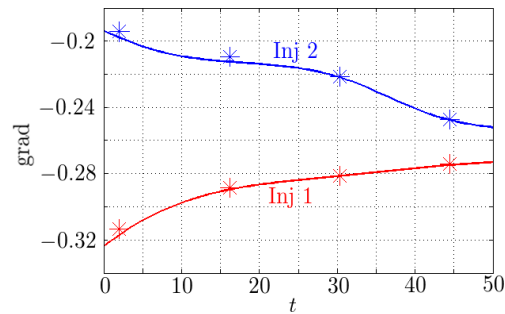


Figure 23: The gradient of  $\xi$  with respect to rates at the two injectors. The lines indicate the gradients estimated by the twin model, while the stars indicate the true gradient evaluated by finite difference.

Error	$t = 0.04$	$t = 0.32$	$t = 0.6$	$t = 0.88$
Inj 1	1.7	1.0	0.6	0.2
Inj 2	2.2	1.9	0.7	0.2

Table 3: The error of estimated gradient at day 2, 16, 30, and 44, in percentage.

## 6. Conclusions

This article develops a method for gradient estimation by using the space-time solution of gray-box conservation law simulations. In particular, an adjoint-enabled twin model is trained to minimize the solution mismatch metric. The inferrability of the twin model is studied theoretically for a simple PDE with only one equation and one dimensional space. To enable the training computationally, a sigmoid parameterization is presented. However, an ad hoc choice for the bases does not fully exploit the information contained in the gray-box solution. To address this issue, an adaptive basis construction procedure is presented. The adaptive procedure builds upon three key elements: the approximated basis significance, the basis neighborhood, and the cross validation. The algorithm for training the twin model is summarized. To alleviate the training cost, a pre-train step is suggested that minimizes the integrated truncation error instead of the solution mismatch.

The proposed twin model algorithm has a wide applicability, which is demonstrated on a variety of numerical examples. The first example is the Buckley-Leverett equation, whose flux function is inferred. The trained twin model accurately estimates the gradient of an objective to the source term. The second example is the steady-state Navier-Stokes equation in a return bend, whose state equation is inferred. The inferred state equation allows estimating the gradient of mass flux to the control surface geometry. The third example is the petroleum reservoir with polymer injection, where the mobility factors are inferred. The gradient of the residual oil to the injection rate is estimated. With the aid of the estimated gradient, the objective can be optimized more efficiently, which will be discussed in a companion paper.

There are several potential thrusts of further research: A useful extension is to investigate the inferrability of twin models for various conservation laws. In particular, Theorem 1 may be extended for problems with a system of equations and higher spatial dimension. Another interesting extension is to study the applicability of the pre-train step, especially to obtain a necessary and sufficient condition for bounding  $\mathcal{M}$  with  $\mathcal{T}$ . Finally, it is interesting to generalize the formulation (2.2) to incorporate unknown source terms and boundary conditions.

## 7. Appendix

### 7.1. Theorem 1

Proof:

We prove false the contradiction of the theorem, which reads:

For any  $\delta > 0$  and  $T > 0$ , there exist  $\epsilon > 0$ , and  $F, \tilde{F}$  satisfying the conditions stated in theorem 1, such that  $\|\tilde{u} - u\|_\infty < \delta$  and  $\left\| \frac{d\tilde{F}}{du} - \frac{dF}{du} \right\|_\infty > \epsilon$  on  $B_u$ .

We show the following exception to the contradiction in order to prove it false.

For any  $\epsilon > 0$  and any  $F, \tilde{F}$  satisfying  $\left\| \frac{d\tilde{F}}{du} - \frac{dF}{du} \right\|_\infty > \epsilon$  on  $B_u$ , we can find  $\delta > 0$  and  $T > 0$  such that  $\|\tilde{u} - u\|_\infty > \delta$ .

The idea is to construct such an exception by the method of lines Schiesser (91). Firstly, assume there is no shock wave for (4.4) and (4.5) for  $t \in [0, T]$ . Choose a segment in space,  $[x_0 - \Delta, x_0]$  with  $0 < \Delta < \frac{\epsilon}{L_F L_u}$ , that satisfies

- $u_0(x) \in B_u$  for any  $x \in [x_0 - \Delta, x_0]$ ;
- $\left| \frac{d\tilde{F}}{du}(u_0(x_0)) - \frac{dF}{du}(u_0(x_0)) \right| > \epsilon$ ;
- $x_0 - \Delta + \frac{dF}{du}(u_0(x_0 - \Delta))T = x_0 + \frac{d\tilde{F}}{du}(u_0)T \equiv x^*$ .

Without loss of generality, we assume  $\frac{dF}{du} > 0$  and  $\frac{d\tilde{F}}{du} > 0$  for  $\{u | u = u_0(x), x \in [x_0 - \Delta, x_0]\}$ . Using the method of lines, we have

$$u \left( T, x_0 - \Delta + \frac{dF}{du}(u_0(x_0 - \Delta))T \right) = u_0(x_0 - \Delta),$$

and

$$\tilde{u} \left( T, x_0 + \frac{d\tilde{F}}{du}(u_0(x_0))T \right) = u_0(x_0).$$

Therefore

$$|\tilde{u}(x^*, T) - u(x^*, T)| = |u_0(x_0) - u_0(x_0 - \Delta)| \geq \gamma \Delta \equiv \delta,$$

by using the definition of  $B_u$ .

Set  $T = \frac{\Delta}{\left| \frac{d\tilde{F}}{du}(u_0(x_0 - \Delta)) - \frac{dF}{du}(u_0(x_0)) \right|}$ , we have

$$\begin{aligned} & \left| \frac{d\tilde{F}}{du}(u_0(x_0 - \Delta)) - \frac{dF}{du}(u_0(x_0)) \right| \\ &= \left| \frac{dF}{du}(u_0(x_0)) - \frac{d\tilde{F}}{du}(u_0(x_0)) + \frac{dF}{du}(u_0(x_0 - \Delta)) - \frac{dF}{du}(u_0(x_0)) \right| \\ &= \left| \frac{dF}{du}(u_0(x_0)) - \frac{d\tilde{F}}{du}(u_0(x_0)) + \frac{d^2 F}{du^2}(u_0(x_0 - \Delta) - u_0(x_0)) \right| \\ &\geq \left| \frac{dF}{du}(u_0(x_0)) - \frac{d\tilde{F}}{du}(u_0(x_0)) \right| - L_u L_F \Delta \\ &\geq \epsilon - L_u L_F \Delta \equiv \epsilon_F > 0 \end{aligned}$$

by using the mean value theorem. Therefore  $T \leq \frac{\Delta}{\epsilon_F} < \infty$ . So we find a  $\delta = \gamma\Delta$  and a  $T < \infty$  that provides an exception to the contradiction of the theorem.

Secondly, if there is shock wave within  $[0, T]$  for either (4.4) or (4.5), we let  $T^*$  be the time of the shock occurrence. Without loss of generality, assume the shock occurs for (4.4) first. The shock implies the intersection of two characteristic lines. Choose a  $\Delta > 0$  such that  $|\frac{dF}{du}(u_0(x)) - \frac{dF}{du}(u_0(x - \Delta))|T^* = \Delta$ . Using the mean value theorem, we have

$$T^* = \frac{\Delta}{\frac{d^2F}{du^2}(u_0(x) - u_0(x - \Delta))} \geq \frac{1}{L_u L_F}$$

Thus, if we choose

$$T = \min \left\{ \frac{1}{L_u L_K}, \frac{\Delta}{\epsilon_\Delta} \right\},$$

no shock occurs in  $t \in [0, T]$ . Since the theorem is already proven for the no-shock scenario, the proof completes.  $\checkmark$

## 7.2. Theorem 2

Proof:

Let the one-step time marching of the gray-box simulator be

$$\mathcal{H} : \mathbb{R}^n \mapsto \mathbb{R}^n, \mathbf{u}_i \rightarrow \mathbf{u}_{i+1} = \mathcal{H}\mathbf{u}_i, \quad i = 1, \dots, M-1,$$

The integrated truncation error can be written as

$$\begin{aligned} \mathcal{T}(\tilde{F}) &= \sum_{i=1}^M \sum_{j=1}^N w_j (\mathbf{u}_{i+1j} - (\mathcal{G}\mathbf{u}_i)_j)^2 \\ &= \sum_{i=1}^M (\mathbf{u}_{i+1\cdot} - \mathcal{G}\mathbf{u}_i)^T W (\mathbf{u}_{i+1\cdot} - \mathcal{G}\mathbf{u}_i) \\ &= \sum_{i=1}^M \|\mathbf{u}_{i+1\cdot} - \mathcal{G}\mathbf{u}_i\|_W^2 \\ &= \sum_{i=1}^M \|\mathcal{H}\mathbf{u}_i - \mathcal{G}\mathbf{u}_i\|_W^2 \\ &= \sum_{i=1}^M \|(\mathcal{H}^i - \mathcal{G}\mathcal{H}^{i-1})\mathbf{u}_0\|_W^2. \end{aligned}$$

Similarly, the solution mismatch can be written as

$$\mathcal{M}(\tilde{F}) = \sum_{i=1}^M \|(\mathcal{H}^i - \mathcal{G}^i)\mathbf{u}_0\|_W^2$$

Fig 24 gives an explanation of  $\mathcal{M}$  and  $\mathcal{T}$  by viewing the simulators as discrete-time dynamical systems.

Using the equality

$$\mathcal{G}^i - \mathcal{H}^i = (\mathcal{G}^i - \mathcal{G}^{i-1}\mathcal{H}) + (\mathcal{G}^{i-1}\mathcal{H} - \mathcal{G}^{i-2}\mathcal{H}^2) + \dots + (\mathcal{G}\mathcal{H}^{i-1} - \mathcal{H}^i), \quad i \in \mathbb{N},$$

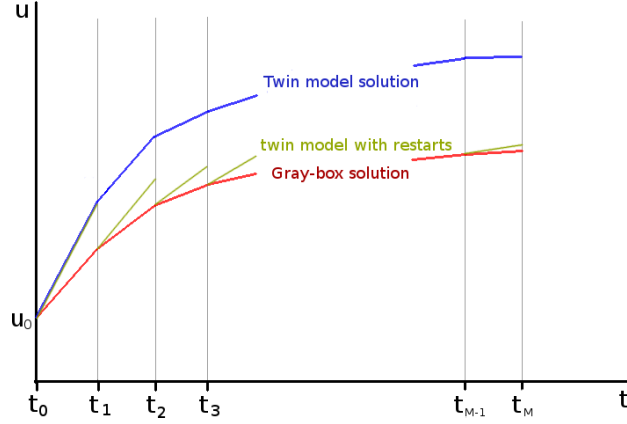


Figure 24: The state-space trajectories of the gray-box model and the twin model.  $\mathcal{M}$  measures the difference of the twin model trajectory (blue) with the gray-box trajectory (red).  $\mathcal{T}$  measures the difference of the twin model trajectory with restarts (green) and the gray-box trajectory (red).

and triangular inequality, we have

$$\mathcal{M} \leq \left\{ \begin{array}{l} \|(\mathcal{G}^{M-1}\mathcal{G} - \mathcal{G}^{M-1}\mathcal{H})u_0\|_{\mathcal{W}}^2 + \|(\mathcal{G}^{M-2}\mathcal{G}\mathcal{H} - \mathcal{G}^{M-2}\mathcal{H}^2)u_0\|_{\mathcal{W}}^2 + \cdots + \|(\mathcal{G}\mathcal{H}^{M-1} - \mathcal{H}^M)u_0\|_{\mathcal{W}}^2 \\ \quad + \|(\mathcal{G}^{M-2}\mathcal{G} - \mathcal{G}^{M-2}\mathcal{H})u_0\|_{\mathcal{W}}^2 + \cdots + \|(\mathcal{G}\mathcal{H}^{M-2} - \mathcal{H}^{M-1})u_0\|_{\mathcal{W}}^2 \\ \quad \quad \quad \vdots \\ \quad \quad \quad + \|(\mathcal{G} - \mathcal{H})u_0\|_{\mathcal{W}}^2 \end{array} \right\}.$$

Therefore,

$$\mathcal{M} - \mathcal{T} \leq$$

$$\left\{ \begin{array}{l} \|(\mathcal{G}^{M-1}\mathcal{G} - \mathcal{G}^{M-1}\mathcal{H})u_0\|_{\mathcal{W}}^2 + \|(\mathcal{G}^{M-2}\mathcal{G}\mathcal{H} - \mathcal{G}^{M-2}\mathcal{H}^2)u_0\|_{\mathcal{W}}^2 + \cdots + \|(\mathcal{G}\mathcal{G}\mathcal{H}^{M-2} - \mathcal{G}\mathcal{H}^{M-1})u_0\|_{\mathcal{W}}^2 \\ \quad + \|(\mathcal{G}^{M-2}\mathcal{G} - \mathcal{G}^{M-2}\mathcal{H})u_0\|_{\mathcal{W}}^2 + \cdots + \|(\mathcal{G}\mathcal{G}\mathcal{H}^{M-3} - \mathcal{G}\mathcal{H}^{M-2})u_0\|_{\mathcal{W}}^2 \\ \quad \quad \quad \vdots \\ \quad \quad \quad + \|(\mathcal{G}\mathcal{G} - \mathcal{G}\mathcal{H})u_0\|_{\mathcal{W}}^2 \end{array} \right\}.$$

Under the assumption

$$\|\mathcal{G}a - \mathcal{G}b\|_{\mathcal{W}}^2 \leq \beta \|a - b\|_{\mathcal{W}}^2,$$

and its implication

$$\|\mathcal{G}^i a - \mathcal{G}^i b\|_{\mathcal{W}}^2 \leq \beta^i \|a - b\|_{\mathcal{W}}^2, \quad i \in \mathbb{N},$$

we have

$$\mathcal{M} - \mathcal{T} \leq \left\{ \begin{array}{l} \beta^{M-1} \|(\mathcal{G} - \mathcal{H})u_0\|_{\mathcal{W}}^2 + \beta^{M-2} \|(\mathcal{G}\mathcal{H} - \mathcal{H}^2)u_0\|_{\mathcal{W}}^2 + \cdots + \beta \|(\mathcal{G}\mathcal{H}^{M-2} - \mathcal{H}^{M-1})u_0\|_{\mathcal{W}}^2 \\ \quad + \beta^{M-2} \|(\mathcal{G} - \mathcal{H})u_0\|_{\mathcal{W}}^2 + \cdots + \beta \|(\mathcal{G}\mathcal{H}^{M-3} - \mathcal{H}^{M-2})u_0\|_{\mathcal{W}}^2 \\ \quad \quad \quad \vdots \\ \quad \quad \quad + \beta \|(\mathcal{G} - \mathcal{H})u_0\|_{\mathcal{W}}^2 \end{array} \right\}.$$





REFERENCES

- RAMIREZ, W.F. Application of Optimal Control Theory to Enhanced Oil Recovery. *Elsevier*, vol. 21, 1987.
- RAMIREZ, W. F., FATHI, Z., AND CAGNOL, J. L. Optimal Injection Policies for Enhanced Oil Recovery: Part 1 Theory and Computational Strategies. *Society of Petroleum Engineers Journal*, 24(03): 328-332, 1984.
- Buckley, S. E., and Leverett, M. Mechanism of Fluid Displacement in Sands. *Transactions of the AIME*, 146(01): 107-116, 1942.
- Peaceman, D. W. Fundamentals of Numerical Reservoir Simulation Vol. 6. *Elsevier*, 2000.
- Alvarado, V., and Manrique, E. Enhanced Oil Recovery: an Update Review. *Energies*, 3(9):1529-1575, 2010.
- Verstraete, T., Coletti, F., Bulle, J., Vanderwielen, T., and Arts, T. Optimization of a U-Bend for Minimal Pressure Loss in Internal Cooling Channels - Part I: Numerical Method. *Journal of Turbomachinery*, 135(5):051015, 2013.
- Coletti, F., Verstraete, T., Bulle, J., Van der Wielen, T., Van den Berge, N., and Arts, T. Optimization of a U-Bend for Minimal Pressure Loss in Internal Cooling Channels - Part II: Experimental Validation. *Journal of Turbomachinery*, 135(5):051016, 2013.
- Redlich, O., and Kwong, J. N. On the Thermodynamics of Solutions. V. An Equation of State. Fugacities of Gaseous Solutions. *Chemical Reviews*, 44(1):233-244, 1949.
- Han, J. C., Dutta, S., and Ekkad, S. Gas Turbine Heat Transfer and Cooling Technology. *CRC Press*, 2012.
- Lions, J.L. Optimal Control of Systems Governed by Partial Differential Equations, vol. 170, *Springer-Verlag*, 1971.
- Jameson, A. Aerodynamic Design via Control Theory, *Journal of Scientific Computing*, 3(3):233-260, 1988.
- Anderson, W. K., and Venkatakrisnan, V. Aerodynamic Design Optimization on Unstructured Grids with a Continuous Adjoint Formulation. *Computers and Fluids*, 28(4):443-480, 1999.
- Renaud, J. E. Automatic Differentiation in Robust Optimization. *AIAA Journal*, 35(6):1072-1079, 1997.
- Plessix, R. E. A Review of the Adjoint-state Method for Computing the Gradient of a Functional with Geophysical Applications. *Geophysical Journal International*, 167(2):495-503, 2006.
- Zandvliet, M., Handels, M., van Essen, G., Brouwer, R., and Jansen, J. D. Adjoint-based Well-placement Optimization under Production Constraints. *SPE Journal*, 13(04):392-399, 2008.
- Giles, M. B., Duta, M. C., M-uacute, J. D., ller, and Pierce, N. A. Algorithm Developments for Discrete Adjoint Methods. *AIAA journal*, 41(2):198-205, 2003.
- Corliss, G. Automatic Differentiation of Algorithms: From Simulation to Optimization. *Springer Science and Business Media*, vol.1, 2002.
- Giles, M. B., and Pierce, N. A. An Introduction to the Adjoint Approach to Design. *Flow, Turbulence and Combustion*, 65(3-4):393-415, 2000.
- Schneider, R. Applications of the Discrete Adjoint Method in Computational Fluid Dynamics. *Doctoral Dissertation, The University of Leeds*, 2006.
- Walther, A. and Griewank, A. Getting Started with ADOL-C. *In U. Naumann und O.*

- Schenk, *Combinatorial Scientific Computing, Chapman-Hall CRC Computational Science*, pp. 181-202, 2012.
- McIlhagga, W. <http://www.mathworks.com/matlabcentral/fileexchange/26807-automatic-differentiation-with-matlab-objects>
- Bergstra, J., Breuleux, O., Bastien, F., Lamblin, P., Pascanu, R., Desjardins, G., Turian, J., Warde-Farley, D., and Bengio, Y. Theano: A CPU and GPU Math Expression Compiler, *Proceedings of the Python for Scientific Computing Conference*, Austin, TX, 2010.
- Ghanem, R. G., and Spanos, P. D. Stochastic Finite Elements: a Spectral Approach. *Courier Corporation*, 2003.
- Smolyak, S. A. Interpolation and Quadrature formulas for the classes  $W_s^a$  and  $E_s^a$ . *Dokl. Akad. Nauk SSSR*, vol.131:1028-1031, 1960.
- Chen, S. S., Donoho, D. L., and Saunders, M. A. Atomic Decomposition by Basis Pursuit. *SIAM Review*, 43(1):129-159, 2001.
- Daubechies, I. Time-frequency Localization Operators: a Geometric Phase Space Approach. *Information Theory, IEEE Transactions on*, 34(4):605-612, 1988.
- Saltelli, A., Chan, K., and Scott, E. M. Sensitivity Analysis vol. 1, New York, Wiley, 2000.
- Mallat, S. G., and Zhang, Z. Matching Pursuits with Time-Frequency Dictionaries. *Signal Processing, IEEE Transactions on*, 41(12):3397-3415, 1993.
- Friedman, J. H. An Overview of Predictive Learning and Function Approximation. *Springer Berlin Heidelberg*, pp. 1-61, 1994.
- Reed, R. Pruning Algorithms - a Survey. *Neural Networks, IEEE Transactions on*, 4(5):740-747, 1993.
- Jekabsons, G. Adaptive Basis Function Construction: an Approach for Adaptive Building of Sparse Polynomial Regression Models. *INTECH Open Access Publisher*, 2010.
- Blatman, G., and Sudret, B. Sparse Polynomial Chaos Expansions and Adaptive Stochastic Finite Elements Using a Regression Approach. *Comptes Rendus Mécanique*, 336(6):518-523, 2008.
- Blatman, G., and Sudret, B. An Adaptive Algorithm to Build up Sparse Polynomial Chaos Expansions for Stochastic Finite Element Analysis. *Probabilistic Engineering Mechanics*, 25(2):183-197, 2010.
- Miller, A. Subset Selection in Regression. *London: Chapman and Hall Press*, 1990.
- Geisser, S. Predictive inference, *CRC press*, vol. 55, 1993.
- Lohmiller, W., and Slotine, J. J. E. On Contraction Analysis for Non-linear Systems. *Automatica*, 34(6):683-696, 1998.
- Dennis, Jr, John E., and Jorge J. Moré. Quasi-Newton Methods, Motivation and Theory. *SIAM Review*, 19(1):46-89, 1977.
- Rios, L. M., and Sahinidis, N. V. Derivative-free Optimization: A Review of Algorithms and Comparison of Software Implementations. *Journal of Global Optimization*, 56(3):1247-1293, 2013.
- Nocedal, J. Updating Quasi-Newton Matrices with Limited Storage. *Mathematics of computation*, 35(151):773-782, 1980.
- Tibshirani, R. Regression Shrinkage and Selection via the Lasso. *Journal of the Royal Statistical Society, Series B (Methodological)*:267-288, 1996.
- Torczon, V. On the Convergence of Pattern Search Algorithms. *SIAM Journal on optimization*, 7(1):1-25, 1997.

- Conn, A. R., Gould, N. I., and Toint, P. L. Trust Region Methods. *SIAM*, vol. 1, 2000.
- Powell, M.J. A Direct Search Optimization Method that Models the Objective and Constraint Functions by Linear Interpolation. *Advances in Optimization and Numerical Analysis*, pp. 51-67, Springer Netherlands, 1994.
- Alexandrov, N.M., Lewis, R.M., Gumbert, C.R., Green, L.L, and Newman, P.A. Approximation and Model Management in Aerodynamic Optimization with Variable Fidelity Models. *AIAA Journal of Aircraft*, 38(6):1093–1101, 2001.
- Conn, A. R., Scheinberg, K., and Vicente, L. N. Global Convergence of General Derivative-free Trust-region Algorithms to First-and Second-order Critical Points. *SIAM Journal on Optimization*, 20(1):387-415, 2009
- Wild, S. M., and Shoemaker, C. Global Convergence of Radial Basis Function Trust-region Algorithms for Derivative-free Optimization. *SIAM Review*, 55(2):349-371, 2013
- Pintér, J.D. Global Optimization in Action: Continuous and Lipschitz Optimization. Algorithms, Implementations and Applications. *Nonconvex Optimization and its Applications*, vol. 6, 1996.
- Schwefel, H. P. P. Evolution and Optimum Seeking: the Sixth Generation. *John Wiley & Sons, Inc.*, 1993.
- Holland, J.H. Adaptation in Natural and Artificial Systems. *The University of Michigan Press*, Ann Arbor, 1975.
- Banks, A., Vincent, J., and Anyakoha, C. A Review of Particle Swarm Optimization. Part I: Background and Development. *Natural Computing*, 6(4):467-484, 2007.
- Yang, X. S., and Deb, S. Engineering Optimisation by Cuckoo Search. *International Journal of Mathematical Modelling and Numerical Optimisation*, 1(4):330-343, 2010.
- Alexandrov, N. M., Dennis Jr, J. E., Lewis, R. M., and Torczon, V. A Trust-region Framework for Managing the Use of Approximation Models in Optimization. *Structural Optimization*, 15(1):16-23, 1998.
- Carter, R. G. On the Global Convergence of Trust Region Algorithms Using Inexact Gradient Information. *SIAM Journal on Numerical Analysis*, 28(1):251-265, 1991.
- Carter, R. G. Numerical Experience with a Class of Algorithms for Nonlinear Optimization Using Inexact Function and Gradient Information. *SIAM Journal on Scientific Computing*, 14(2):368-388, 1993.
- Fu, M. C. Optimization via Simulation: A Review. *Annals of Operations Research*, 53(1):199-247, 1994.
- OpenFOAM, <http://www.openfoam.org/>
- Aspen, <http://www.aspentech.com/products/aspenONE/>
- Chen, W., Xiong, Y., Tsui, K. L., and Wang, S. A Design-driven Validation Approach Using Bayesian Prediction Models. *Journal of Mechanical Design*, 130(2):021101, 2008.
- Wang, S., Tsui, K. L., and Chen, W., Bayesian Validation of Computer Models. *Technometrics*, 51(4):439–451, 2009.
- Qian, P. Z., and Wu, C. J. Bayesian Hierarchical Modeling for Integrating Low-accuracy and High-accuracy Experiments. *Technometrics*, 50(2):192-204, 2008.
- Zhou, D. X. Derivative Reproducing Properties for Kernel Methods in Learning Theory. *Journal of computational and Applied Mathematics*, 220(1):456-463, 2008
- Vazquez, E., and Bect, J. Convergence Properties of the Expected Improvement Algo-

- rithm with Fixed Mean and Covariance Functions. *Journal of Statistical Planning and inference*, 140(11):3088-3095, 2010.
- Bull, A. D. Convergence Rates of Efficient Global Optimization Algorithms. *The Journal of Machine Learning Research* 12:2879-2904, 2011.
- Srinivas, N., Krause, A., Kakade, S. M., and Seeger, M. Gaussian Process Optimization in the Bandit Setting: No Regret and Experimental Design. *arXiv preprint arXiv:0912.3995*, 2009
- Berlinet, A., and Thomas-Agnan, C. Reproducing Kernel Hilbert Spaces in Probability and Statistics. *Springer Science and Business Media*, 2011.
- Snoek, J., Larochelle, H., and Adams, R. P. Practical Bayesian Optimization of Machine Learning Algorithms. *Advances in Neural Information Processing Systems*. pp.2951-2959, 2012
- Močkus, J., Tiesis, V., and Zilinskas, A. The Application of Bayesian Methods for Seeking the Extremum. *Towards Global Optimization* 2(117-129), 1978.
- Locatelli, M. Bayesian Algorithms for One-dimensional Global Optimization. *Journal of Global Optimization*, 10(1):57-76, 1997.
- Chung, H. S., and Alonso, J. J. Using Gradients to Construct CoKriging Approximation Models for High-dimensional Design Optimization Problems. *American Institute of Aeronautics and Astronautics paper*, 992, 2001.
- Vauclin, M., Vieira, S. R., Vachaud, G., and Nielsen, D. R. The Use of CoKriging with Limited Field Soil Observations. *Soil Science Society of America Journal*, 47(2):175-184, 1983
- Kennedy, M. C., and O'Hagan, A. Predicting the Output from a Complex Computer Code when Fast Approximations are Available. *Biometrika*, 87(1):1-13, 2000.
- Kennedy, M. C., and O'Hagan, A. Bayesian Calibration of Computer Models. *Journal of the Royal Statistical Society: Series B (Statistical Methodology)*, 63(3):425-464, 2001.
- Higdon, D., Kennedy, M., Cavendish, J. C., Cafoe, J. A., and Ryne, R. D. Combining Field Data and Computer Simulations for Calibration and Prediction. *SIAM Journal on Scientific Computing*, 26(2):448-466, 2004.
- O'Hagan, A. A Markov Property for Covariance Structures. *Statistics Research Report*, 98(13), 1998.
- Aronszajn, N. Theory of Reproducing Kernels. *Transactions of the American Mathematical Society*, 68(3):337-404, 1950.
- Showalter, R. E. Hilbert Space Methods for Partial Differential Equations. *Dover Publications*, Mineola, New York, 2010
- Jones, D. R., Schonlau, M., and Welch, W. J. Efficient Global Optimization of Expensive Black-box Functions. *Journal of Global Optimization*, 13(4):455-492, 1998.
- Bertsekas, D. P. Nonlinear Programming. *Athena Scientific*, Cambridge, MA, 1999.
- Spall, J. C. Introduction to Stochastic Search and Optimization: Estimation, Simulation, and Control. *John Wiley & Sons*, vol. 65, 2005.
- Fletcher, R., and Reeves, C. M. Function Minimization by Conjugate Gradients. *The Computer Journal*, 7(2):149-154, 1964.
- Dai, Y. H., and Yuan, Y. A Nonlinear Conjugate Gradient Method with a Strong Global Convergence Property. *SIAM Journal on Optimization*, 10(1):177-182, 1999.
- Gudmundsson, S. Parallel Global Optimization. *Master Thesis*, IMM, Technical University of Denmark, 1998.

- Žilinskas, J. Branch and Bound with Simplicial Partitions for Global Optimization. *Mathematical Modelling and Analysis*, 13(1):145-159, 2008.
- Noel, M. M. A New Gradient Based Particle Swarm Optimization Algorithm for Accurate Computation of Global Minimum. *Applied Soft Computing*, 12(1):353-359, 2012.
- Yang, X. S., and Deb, S. Cuckoo Search: Recent Advances and Applications. *Neural Computing and Applications*, 24(1):169-174, 2014.
- Rasmussen, C. E. Gaussian Processes in Machine Learning. in *Advanced Lectures on Machine Learning*, Springer Berlin Heidelberg, pp.63-71, 2004.
- Matérn, B. Spatial Variation, *Springer*, New York, 1960.
- Kushner, H. J. A New Method of Locating the Maximum Point of an Arbitrary Multipeak Curve in the Presence of Noise. *Journal of Basic Engineering*, 86(1):97-106, 1964.
- Chen, H. Black-box Stencil Interpolation Method for Model Reduction. *Master thesis*, Department of Aeronautics and Astronautics, Massachusetts Institute of Technology, 2012.
- Schiesser, W. E. The Numerical Methods of Lines. *Academic Press*, 1991.
- Mallat, S. G. A Theory for Multiresolution Signal Decomposition: the Wavelet Representation. *Pattern Analysis and Machine Intelligence, IEEE Transactions on*, 11(7):674-693, 1989.
- Murdock, J. W. Fundamental Fluid Mechanics for the Practicing Engineer, *CRC Press*, 1993.
- Armijo, L. Minimization of Functions Having Lipschitz Continuous First Partial Derivatives. *Pacific Journal of Mathematics*, 16(1):1-3, 1966.
- Taylor, A. E., and Lay, D. C. Introduction to Functional Analysis. *vol. 2, Wiley, New York*, 1958.
- Anslys Fluent Theory Guide. *ANSYS Inc.*, USA, 2011.
- ANSYS CFX-solver Theory Guide. *ANSYS CFX Release*, 11, 69-118, 2012.